bioRxiv preprint doi: https://doi.org/10.1101/227264; this version posted November 30, 2017. The copyright holder for this preprint (which was not certified by peer review) is the author/funder, who has granted bioRxiv a license to display the preprint in perpetuity. It is made available under aCC-BY 4.0 International license.

An Essential Role for Argonaute 2 in EGFR-KRAS Signaling in Pancreatic Cancer Development

Sunita Shankar[1,2,*], Jean Ching-Yi Tien[1,2,*], Ronald F. Siebenaler[1,2], Vijaya L. Dommeti[1,2], Sylvia Zelenka-Wang[1,2], Kristin M. Juckette[1,2], Alice Xu[1,2], Malay Mody[1,2], Andrew Goodrum[1,2], Grace Tsaloff[1,2], Ingrid J. Apel[1,2], Lisha Wang[1,2], Javed Siddiqui[1,2], Jiaqi Shi[2], Chandan Kumar-Sinha[1,2], Arul M. Chinnaiyan[1,2,3,4,5].

1 Michigan Center for Translational Pathology, University of Michigan, Ann Arbor, Michigan 48109, USA
2 Department of Pathology, University of Michigan, Ann Arbor, Michigan 48109, USA
3 Howard Hughes Medical Institute, University of Michigan, Ann Arbor, Michigan 48109, USA
4 Department of Urology, University of Michigan, Ann Arbor, Michigan 48109, USA
5 Comprehensive Cancer Center, University of Michigan, Ann Arbor, Michigan 48109, USA

*These authors contributed equally to this work.

Key words: pancreatic cancer, KRAS, EGFR, EIF2C2, Argonaute 2, RNA silencing

Corresponding Author

Arul M. Chinnaiyan, M.D., Ph.D.
Investigator, Howard Hughes Medical Institute
American Cancer Society Professor
S. P. Hicks Endowed Professor of Pathology
Professor of Pathology and Urology
Comprehensive Cancer Center
University of Michigan Medical School
1400 E. Medical Center Dr. 5316 CCGC
Ann Arbor, MI 48109-0602
arul@umich.edu

bioRxiv preprint doi: https://doi.org/10.1101/227264; this version posted November 30, 2017. The copyright holder for this preprint (which was not certified by peer review) is the author/funder, who has granted bioRxiv a license to display the preprint in perpetuity. It is made available under aCC-BY 4.0 International license.

KRAS **and** ***EGFR*** **have been shown to function as essential mediators of pancreatic cancer development[1-4]. In addition,** ***KRAS*** **and** ***EGFR*** **have been shown to interact with and perturb the function of Argonaute 2 (AGO2), a key mediator of RNA-mediated gene silencing[5,6]. Here, we employed a genetically engineered mouse model of pancreatic cancer[7,8] to define the effects of conditional loss of** ***AGO2*** **in** ***KRAS^{G12D}*** **driven pancreatic cancer. Genetic ablation of** ***AGO2*** **does not interfere with development of the normal pancreas or** ***KRAS^{G12D}*** **driven early precursor pancreatic intraepithelial (PanIN) lesions. However,** ***AGO2*** **loss prevents progression from early to late PanIN lesions, development of pancreatic ductal adenocarcinoma (PDAC), and metastatic progression. This results in a dramatic increase in survival of** ***KRAS^{G12D}*** **mutant mice deficient in AGO2 expression. In both mouse and human pancreatic tissues, increased AGO2 expression at the plasma membrane is associated with PDAC progression. Mechanistically, within early precursor PanIN lesions, loss of AGO2 elevates phospho-EGFR levels and activates wild-type RAS, antagonizing** ***KRAS^{G12D}*** **activation and PDAC development. Furthermore, we observe that phosphorylation of AGO2^{Y393} by EGFR[6] disrupts the interaction of wild-type RAS with AGO2, but does not affect the interaction of mutant KRAS with AGO2. Taken together, our study supports a biphasic model of pancreatic cancer development: an AGO2-independent early phase of PanIN formation reliant on EGFR and wild-type RAS signaling, and an AGO2-dependent phase wherein the KRAS-AGO2 interaction is critical to the progression from PanIN to PDAC.**

bioRxiv preprint doi: https://doi.org/10.1101/227264; this version posted November 30, 2017. The copyright holder for this preprint (which was not certified by peer review) is the author/funder, who has granted bioRxiv a license to display the preprint in perpetuity. It is made available under aCC-BY 4.0 International license.

Mutations in *RAS* account for over 30% of all cancers and over 90% of pancreatic cancer harbor *KRAS* mutations, a disease with a dismal overall 5-year survival rate of only 7%[9]. The KRAS GTPase transduces extracellular mitogenic signals by cycling between an active GTP-bound and an inactive GDP-bound state. Recurrent driver mutations in KRAS decrease intrinsic GTPase activity thereby accumulating in its active GTP-bound form. Constitutively active KRAS leads to aberrant signaling activities through interactions with multiple effector proteins[10-12]. Recently, we identified an interaction between KRAS and Argonaute 2 (AGO2), independent of *KRAS* mutation status[5] and similarly Shen et al identified a functional interaction between EGFR and AGO2[6]. Here we employ an established mouse model of pancreatic cancer to explore the *in vivo* requirement of AGO2 in pancreatic cancer development in the context of KRAS and EGFR signaling.

To investigate the role of *AGO2* in the development of pancreatic cancer *in vivo*, we interrogated the genetically engineered mouse model of pancreatic cancer initiated by a conditionally activated allele of KRAS[7], LSL-$KRAS^{G12D}$ ($KRAS^{G12D}$, shown in **Fig. 1a**). Crossing $KRAS^{G12D}$ mice with animals harboring *Cre* recombinase under the control of pancreatic acinar cell-specific promoter, *p48* (*p48Cre*), yields $KRAS^{G12D}$*;p48Cre* mice that develop pancreatic intraepithelial precursor lesions (PanINs) within 3 weeks of age[7]. Over time, these PanINs progress to pancreatic adenocarcinoma (PDAC) and develop metastases, faithfully mimicking the human disease. In order to evaluate the potential consequences of *AGO2* ablation in this model, we generated transgenic mice with both $Kras^{G12D}$ and conditionally abrogated allele(s) of *AGO2*[13] (**Fig. 1a**). The resulting $KRAS^{G12D}$*;p48Cre* mice were either wild-type, heterozygous or homozygous for the conditionally expressed allele of *AGO2* (hereafter referred to as $AGO2^{+/+}$*;*$KRAS^{G12D}$*;p48Cre*, $AGO2^{fl/+}$*;*$KRAS^{G12D}$*;p48Cre* and $AGO2^{fl/fl}$*;*$KRAS^{G12D}$*;p48Cre* respectively). Genomic PCR confirmed Cre-driven excision and recombination of the oncogenic KRAS allele[7] in pancreas from mice with $KRAS^{G12D}$*;p48Cre* alleles (**Extended Data Fig. 1a**). Further, qRT-PCR analysis showed significant reduction in AGO2 expression in

bioRxiv preprint doi: https://doi.org/10.1101/227264; this version posted November 30, 2017. The copyright holder for this preprint (which was not certified by peer review) is the author/funder, who has granted bioRxiv a license to display the preprint in perpetuity. It is made available under aCC-BY 4.0 International license.

AGO2$^{fl/fl}$*;KRAS*^{G12D}*;p48Cre* mice (**Extended Data Fig. 1b**), confirming Cre-mediated mutant KRAS activation with concomitant loss of AGO2 expression in the pancreas.

Histological analysis of the pancreas from mice with Cre-mediated *AGO2* ablation (*AGO2*$^{fl/fl}$; *p48Cre*), showed normal morphology (**Fig. 1b**, left panels) with no differences in pancreatic weight compared to pancreata from *AGO2*$^{+/+}$; *p48Cre* mice **(Extended Data Fig. 2)**. This suggests that loss of *AGO2* in the acinar cells of the exocrine compartment, does not interfere with gross pancreas development. Immunohistochemical (IHC) staining with antibodies specific to AGO2 (**Extended Data Fig. 3 and Extended Data Table 1**) showed minimal expression of AGO2 in the acinar and ductal cells of both *AGO2*$^{+/+}$; *p48Cre* and *AGO2*$^{fl/fl}$; *p48Cre* pancreata (**Fig. 1b**, right panels). Interestingly, relatively higher expression of AGO2 was seen in pancreatic endocrine cells (islets of Langerhans), which was unaffected by the acinar cell-specific ablation of *AGO2*. These data indicate a non-essential role for *AGO2* in the acinar cells for normal pancreatic development. However, expression of *KRAS*^{G12D} in the pancreatic acinar cells led to increased AGO2 expression in the PanINs as well as the surrounding stroma in 12 week old *AGO2*$^{+/+}$*;KRAS*^{G12D}*;p48Cre* mice (**Fig. 1c**, top panels). Notably, we observed PanIN lesions in *AGO2*$^{fl/fl}$*;KRAS*^{G12D}*;p48Cre* pancreas lacking AGO2 expression (**Fig. 1c**, lower panels). These early stage precursor PanIN lesions in *AGO2*$^{fl/fl}$*;KRAS*^{G12D}*;p48Cre* pancreas were morphologically indistinguishable from those arising in *AGO2*$^{+/+}$*;KRAS*^{G12D}*;p48Cre* mice. Curiously, while PanIN lesions in *AGO2*$^{fl/fl}$*;KRAS*^{G12D}*;p48Cre* mice fail to exhibit detectable AGO2, the surrounding stromal cells continue to express relatively high levels of AGO2. Further, PanINs from both *AGO2*$^{+/+}$*;KRAS*^{G12D}*;p48Cre* and *AGO2*$^{fl/fl}$*;KRAS*^{G12D}*;p48Cre* mice displayed high mucin content as seen by Alcian blue staining[14] and similar pancreatic weights, indicating indistinct phenotypes at the 12-week time point (**Extended Data Fig. 4**).

Surprisingly, over a longer course of time, mice aged over 400 days (57 weeks) showed significantly increased pancreatic weights in both the *AGO2*$^{+/+}$*;KRAS*^{G12D}*;p48Cre* and

bioRxiv preprint doi: https://doi.org/10.1101/227264; this version posted November 30, 2017. The copyright holder for this preprint (which was not certified by peer review) is the author/funder, who has granted bioRxiv a license to display the preprint in perpetuity. It is made available under aCC-BY 4.0 International license.

AGO2$^{fl/+}$*;KRAS*^{G12D}*;p48Cre* cohort compared to *AGO2*$^{fl/fl}$*;KRAS*^{G12D}*;p48Cre* mice, indicative of a higher tumor burden in mice with at least one functional allele of AGO2 (**Fig. 1d**). Histological analysis of pancreata at the 400 day time point shows early/late PanIN lesions and some PDAC development in *AGO2*$^{+/+}$*;KRAS*^{G12D}*;p48Cre* and *AGO2*$^{fl/+}$*;KRAS*^{G12D}*;p48Cre* mice with a distribution consistent with those reported previously[4,15]. However, in the *AGO2*$^{fl/fl}$*;KRAS*^{G12D}*;p48Cre* mice, mostly early stage PanIN lesions were observed, with no evidence of PDAC (**Fig. 1e**). Occasionally, higher grade PanIN lesions were observed in *AGO2*$^{fl/fl}$*;KRAS*^{G12D}*;p48Cre* pancreata, but these lesions invariably showed AGO2 expression (**Extended Data Fig. 5**), indicative of likely escape from Cre recombination as noted previously in other contexts [4,16]. In order to determine the effect of *AGO2* loss on tumor-free survival, a cohort of transgenic mice was monitored over 500 days. Twelve of 12 *AGO2*$^{+/+}$*;KRAS*^{G12D}*;p48Cre* and 18 of 19 *AGO2*$^{fl/+}$*;KRAS*^{G12D}*;p48Cre* mice died over a median of 406 and 414 days respectively, typical for a murine model expressing *KRAS*^{G12D} in the pancreas[8,17,18]. Remarkably, however, all 12 of 12 mice with homozygous AGO2 deficiency (*AGO2*$^{fl/fl}$*;KRAS*^{G12D}*;p48Cre)* had survived at the cut-off time point of 500 days (**Fig. 1f**). PDAC was observed in pancreata of all mice that express AGO2 (wild type or heterozygous expression) but mice deficient for *AGO2* developed only early PanIN precursor lesions without progression to PDAC (**Fig. 1g**). Necropsy of experimental mice from the different genotypes were also assessed for grossly visible metastases and abnormal pathologies[19] and revealed frequent metastases in the *AGO2*$^{+/+}$*;KRAS*^{G12D}*;p48Cre* and *AGO2*$^{fl/+}$*;KRAS*^{G12D}*;p48Cre* genotypes, but mice from *AGO2*$^{fl/fl}$*;KRAS*^{G12D}*;p48Cre* rarely showed abnormal pathologies, and never frank adenocarcinoma or metastases (**Fig. 1g**). While all metastatic lesions from mice expressing AGO2 showed PDAC, analysis of lungs with abnormal pathologies in two of the *AGO2*$^{fl/fl}$*;KRAS*^{G12D}*;p48Cre* mice (marked as gray boxes) showed a single benign lesion each, associated with AGO2 expression (representing lesions with non-recombined alleles/non pancreatic origin) without indication of PDAC (**Extended Data Table 2** and **Extended Data Fig.**

bioRxiv preprint doi: https://doi.org/10.1101/227264; this version posted November 30, 2017. The copyright holder for this preprint (which was not certified by peer review) is the author/funder, who has granted bioRxiv a license to display the preprint in perpetuity. It is made available under aCC-BY 4.0 International license.

6). One mouse of the *AGO2*$^{fl/fl}$*;KRAS*^{G12D}*;p48Cre* genotype developed a pancreatic cyst (without AGO2 expression), histologically resembling the mucinous cystic neoplasm and survived for 368 days (**Extended Data Table 2** and **Extended Data Fig. 6**). Taken together, these data suggest that *AGO2* is not essential for either normal pancreatic development or *KRAS*^{G12D} driven PanIN formation, however *AGO2* is indispensable for progression of PanIN to PDAC.

Consistent with a role of AGO2 in KRAS driven oncogenesis in the *AGO2*$^{+/+}$*;KRAS*^{G12D}*;p48Cre* mice, IHC analysis showed increased levels of AGO2 in PDAC and metastatic tissues as compared to early PanIN lesions (**Fig. 2a**). This suggests that AGO2 protein levels are elevated with disease progression. To extend these analyses to human pancreatic cancer, we performed a systematic IHC analysis of a human pancreatic tissue microarray (TMA), containing 44 duplicated pancreatic tissue cores, including PanIN, PDAC and metastatic PDAC samples. We observed a remarkable increase in AGO2 expression in PDAC and metastatic PDAC cells compared to PanINs (**Fig. 2b**), scored as statistically significant (**Fig. 2c**). Furthermore, AGO2 staining appeared to be particularly intense along the membranes of PDAC and metastatic PDAC cells, potentially consistent with proximity to KRAS at the plasma membrane[20]. To specifically test this, we performed dual immunofluorescence (IF) staining for AGO2 and KRAS on a pancreatic TMA. As expected, both KRAS specific and pan-RAS antibodies showed positive staining at the membrane. Consistent with our hypothesis, significant AGO2 staining was noted at the plasma membranes of human PDAC and metastatic PDAC cells, where it co-localized with KRAS (**Fig. 2d** and **Extended Data Fig. 7**). These observations support the notion that *in vivo,* AGO2 and KRAS interact at the plasma membrane, the main locus of RAS activity[12,20].

Since the KRAS-AGO2 interaction was previously shown to result in the attenuation of AGO2-mediated gene silencing potentiating oncogenic KRAS driven cellular transformation, here we sought to explore if AGO2 and RAS cooperate mechanistically to drive pancreatic cancer *in vivo*. Earlier, using cell line models we observed that mutant KRAS, but not wild-type

bioRxiv preprint doi: https://doi.org/10.1101/227264; this version posted November 30, 2017. The copyright holder for this preprint (which was not certified by peer review) is the author/funder, who has granted bioRxiv a license to display the preprint in perpetuity. It is made available under aCC-BY 4.0 International license.

RAS reduced the levels of tumor suppressor microRNAs like the *let-7* family members and elevated levels of oncogenic microRNA like *mir-221*[5]. Here, we performed qRT-PCR analysis to interrogate expression levels of over 300 microRNAs from pancreata of *AGO2*$^{+/+}$*;KRAS*^{G12D}*;p48Cre* and *AGO2*$^{fl/fl}$*;KRAS*^{G12D}*;p48Cre* mice, using *AGO2*$^{+/+}$*;p48Cre* as reference. Interestingly, microRNA expression profiles of PanIN lesions with or without AGO2 expression were similar to each other- altogether distinct from normal pancreas (**Extended Data Fig. 8a**). Of note, the *let-7* family tumor suppressor microRNAs[21] were downregulated and the oncogenic *miR-21* levels were upregulated, to the same extent in all PanINs regardless of AGO2 expression, suggesting that microRNA regulation by *KRAS*^{G12D} phenocopies *AGO2* loss (**Extended Data Fig. 8b**). Thus, microRNA regulation *per se* does not account for progression of PanINs to PDAC. This is consistent with previous observations that changes in microRNA profiles alone do not dictate mutant KRAS oncogenesis[22]. Further, in an orthogonal analysis, we investigated if the endonuclease activity of *AGO2*[23] was essential to promote *KRAS*^{G12D} oncogenesis. *In vitro* foci formation assays were performed in *AGO2*$^{-/-}$ NIH3T3 cells using *KRAS*^{G12D} co-transfected with different *AGO2* mutants[5]. As seen in **Extended Data Fig. 9**, both the wild type *AGO2* and slicer deficient *AGO2*^{E637A} mutant[24], but not the RAS-binding deficient[5] double mutant, *AGO2*$^{K112A/E114A}$ efficiently potentiated *KRAS*^{G12D} driven foci formation. Together, these data suggest that while the RAS-AGO2 interaction is critical, AGO2-mediated RISC activity is not required for *KRAS*^{G12D} driven pancreatic cancer.

Next, we sought to explore if AGO2-mediated alteration of RAS signaling in the early stage PanINs could account for the lack of progression to PDAC in the *AGO2*$^{fl/fl}$*;KRAS*^{G12D}*;p48Cre mice*. For this, we specifically focused on EGFR-RAS signaling for two reasons: 1) EGFR has been shown to be essential for PanIN formation in the KRASG12D driven pancreatic mouse model that we have used[3,4,25] and 2) EGFR activation has been shown to directly inhibit AGO2 function through phosphorylation of its Tyr393 residue[6]. Immunoblot analysis of pancreatic tissues from 12-week old mice with *AGO2*$^{+/+}$*;KRAS*^{G12D}*;p48Cre*,

bioRxiv preprint doi: https://doi.org/10.1101/227264; this version posted November 30, 2017. The copyright holder for this preprint (which was not certified by peer review) is the author/funder, who has granted bioRxiv a license to display the preprint in perpetuity. It is made available under aCC-BY 4.0 International license.

AGO2$^{fl/+}$*;KRAS*^{G12D}*;p48Cre* and *AGO2*$^{fl/fl}$*;KRAS*^{G12D}*;p48Cre* genotypes showed markedly elevated phospho-EGFR (Y1068) levels in tissues with AGO2 ablation (**Fig. 3a** and **Extended Data Fig. 10**), indicating activated EGFR signaling. Further, IHC analysis showed that the elevated phospho-EGFR levels observed in tissue lysates were restricted to the PanIN lesions of the pancreas in *AGO2*$^{fl/fl}$*;KRAS*^{G12D}*;p48Cre* mice (**Fig. 3b**). Immunoblots also showed that EGFR activation was accompanied with a remarkable increase in total RAS levels, however, without significant changes in the expression of oncogenic KRAS^{G12D} (**Fig. 3a** and **Extended Data Fig. 10**), raising an intriguing possibility that in early stage PanINs growth factor activation involves signaling along the EGFR-wild-type RAS axis. To investigate this further, we isolated pancreatic ducts from 12 week old *AGO2*$^{+/+}$*;KRAS*^{G12D}*;p48Cre* and *AGO2*$^{fl/fl}$*;KRAS*^{G12D}*;p48Cre* and cultured them as organoids[26], in the absence of EGF (**Extended Data Fig. 11**). Immunoblot analysis showed increased levels of phospho-EGFR and total RAS in the organoids with AGO2 loss, while KRASG12D expression showed no change (**Fig. 3c**), mirroring the observations from pancreatic tissue lysates. Furthermore, analysis of RAS activation displayed higher levels of KRASG12D-GTP in the organoids expressing AGO2 compared to those lacking AGO2. Remarkably, the total RAS levels (which includes both wild-type and mutant RAS) as well as total RAS-GTP was higher in organoids deficient in AGO2. The increased fraction of activated wild-type RAS was accompanied with reduced proliferation rate observed in the organoids with AGO2 loss as compared to AGO2 intact organoids (**Fig. 3d**). These data suggest that loss of AGO2 reduces mutant KRAS function, through activation of wild-type RAS; this is consistent with the tumor suppressor-like function attributed to wild-type RAS[15,27,28]. Importantly, this data also identifies a previously unknown role for AGO2 in limiting wild-type RAS activation through feedback regulation of EGFR in mutant KRAS expressing cells. To probe if AGO2 loss can activate wild type RAS in the absence of mutant KRAS, we performed immunoblot analysis and RAS activation assays using AGO2$^{-/-}$ mouse embryonic fibroblasts (MEFs)[29] that do not harbor any form of oncogenic RAS. As seen in **Fig. 3e**, AGO2 null MEFs also show increased

bioRxiv preprint doi: https://doi.org/10.1101/227264; this version posted November 30, 2017. The copyright holder for this preprint (which was not certified by peer review) is the author/funder, who has granted bioRxiv a license to display the preprint in perpetuity. It is made available under aCC-BY 4.0 International license.

phospho-EGFR and wild type RAS levels along with elevated wild type RAS-GTP levels, and the activation of downstream signaling through ERK and AKT. This signaling cascade is significantly reduced in the same cells rescued with AGO2. Given that AGO2 is a direct phosphorylation substrate of the EGFR kinase[6], our experiments detailed in **Fig. 3**, define a previously unknown reverse feedback regulation of EGFR via AGO2 that controls wild type RAS activation[30-33]. Since AGO2 loss prevents PanIN to PDAC progression, the active EGFR-wild type RAS signaling likely interferes with mutant KRAS function.

Considering that the pancreatic mouse model with loss of AGO2 expression shows activation of both EGFR and wild-type RAS (**Fig. 3**), we posited that AGO2 binding to KRAS may represent a rate limiting step in the activation of wild-type KRAS during growth factor stimulation. To explore this premise, we assayed a panel of cell lines expressing wild-type or mutant RAS, stimulated with EGF, for the KRAS-AGO2 interaction. Interestingly, EGF stimulation resulted in a dramatic reduction in KRAS-AGO2 binding in cells with wild-type KRAS, as assessed in MCF-7, PC3, A375 and HeLa cells (**Fig. 4a** and **Extended Fig. 12**). However, EGF stimulation in cells harboring oncogenic KRAS, including A549 ($KRAS^{G12S}$), MIA Paca-2 ($KRAS^{G12C}$) and Capan-1 ($KRAS^{G12V}$) retained binding of endogenous KRAS and AGO2, despite activation of the EGFR/MAPK pathway (**Fig. 4b**). The disruption of the wild-type RAS-AGO2 interaction was also observed when HEK293 ($KRAS^{WT}$) cells expressing FLAG-tagged AGO2 were stimulated with EGF; the interaction was rescued by treatment of these cells with the EGFR kinase inhibitor, erlotinib (**Fig. 4c**). This strongly suggested that EGFR kinase activity was critical for the disruption of the wild-type KRAS-AGO2 interaction. In contrast, DLD-1 cells harboring mutant $KRAS^{G13D}$, neither EGFR kinase activation by EGF nor its inhibition by erlotinib altered the association of KRAS and AGO2 (**Fig. 4d**). To test if the previously identified phosphorylation of AGO2 by EGFR at tyrosine 393[6] has a role in binding to KRAS, we tested the ability of a phosphorylation deficient $AGO2^{Y393F}$ mutant to bind RAS under different conditions. In HEK293 ($KRAS^{WT}$) cells, EGF stimulation led to dissociation of wild-type AGO2

bioRxiv preprint doi: https://doi.org/10.1101/227264; this version posted November 30, 2017. The copyright holder for this preprint (which was not certified by peer review) is the author/funder, who has granted bioRxiv a license to display the preprint in perpetuity. It is made available under aCC-BY 4.0 International license.

from RAS but the AGO2^{Y393F} mutant continued to bind RAS with or without EGFR activation (**Fig. 4e**). However, expression of these AGO2 constructs in MIA Paca-2 (*KRAS*^{G12S}) cells showed no discernible change in RAS binding upon EGFR activation (summarized in **Fig. 4f**). Together, these data suggest that the wild-type KRAS-AGO2 interaction is sensitive to EGFR mediated phosphorylation of AGO2^{Y393} while the oncogenic KRAS-AGO2 interaction is resistant to both EGFR activation as well as AGO2^{Y393} phosphorylation.

Genetically engineered mouse models have been extensively used to mirror the stepwise progression of human pancreatic cancer, starting with the benign precursor lesion (PanINs) driven by mutant KRAS[8,34,35]. In this study we demonstrate that genetic loss of AGO2 locks KRAS induced pancreatic cancer development in the PanIN stage. AGO2 expression is seen as a critical requirement for progression of PanIN to PDAC. In the absence of AGO2, even the formation of alternate precursor lesions and anaplastic PDAC are not observed, which are described as bypass routes to oncogenesis as noted with *NOTCH2* loss[36]. Progression from PanIN to PDAC also does not require the microRNA-mediated RNA silencing function of AGO2 and likely explains why overlapping RISC activities of other Argonaute family members[37] fail to compensate for AGO2 loss. AGO2 ablation in the PanINs decreases *let-7* microRNA levels and increases EGFR activation together accounting for both elevated wild-type RAS levels[38] and RAS activation[30,31]. Taken together, our data is consistent with previous reports that PanIN development triggered by oncogenic KRAS involves a phase of EGFR activation leading to wild-type RAS signaling. Further progression to PDAC, requires the mutant KRAS-AGO2 interaction, accompanied with reduced EGFR expression[4] and decreased wild-type RAS levels and activity. This nexus between EGFR, wild-type RAS and AGO2 is further supported by our observation that EGF stimulation disrupts the wild-type KRAS-AGO2 interaction, but not the oncogenic KRAS-AGO2 interaction (**Fig. 4f**). It is intriguing that EGFR mediated phosphorylation of AGO2 Y393 disrupts wild-type RAS binding much like AGO2-Dicer binding[6], but AGO2-mutant KRAS binding is immune to AGO2 phosphorylation status. Phosphorylation of AGO2 by EGFR

bioRxiv preprint doi: https://doi.org/10.1101/227264; this version posted November 30, 2017. The copyright holder for this preprint (which was not certified by peer review) is the author/funder, who has granted bioRxiv a license to display the preprint in perpetuity. It is made available under aCC-BY 4.0 International license.

simultaneously inhibits the last step of microRNA biogenesis[6] and activates RAS at the plasma membrane[39], a previously unrecognized aspect of EGF-RAS-MAPK signaling. Yet, disruption of various protein-protein interactions through EGFR phosphorylation[40-42] is a common strategy to modulate the extent of RAS activation signals at the membrane. Regulation of the RAS-AGO2 interaction through growth factor activation also allows the RAS-AGO2 interaction to remain agnostic to the nucleotide (GDP/GTP) binding status of RAS[5]. This is strikingly different from other RAS interactors like RAF, SOS and NF1[11,43], which display preferential binding to GDP or GTP loaded forms of KRAS. EGFR regulation remains limited to the wild type RAS-AGO2 interaction since mutant KRAS, with its reduced rate of GTP hydrolysis, remains constitutively active, bound to AGO2 and refractory to mitogenic stimulation. Finally, we predict that there is an absolute requirement for AGO2 in human PDAC development and that an unregulated oncogenic KRAS-AGO2 interaction at the plasma membrane drives progression of this lethal disease.

Figure Legends

Figure 1 *AGO2* is essential for progression of precursor PanIN lesions to PDAC. a, Schematic of the conditionally activated endogenous alleles of *KRAS^{G12D}* and *AGO2* used in the study to generate the *AGO2$^{fl/fl}$;KRAS^{G12D};p48Cre* experimental mice. **b**, Representative images of H&E and AGO2 IHC analysis of pancreata obtained from *AGO2$^{+/+}$;*p48*Cre* and *AGO2$^{fl/fl}$;p48Cre* genotypes. Orange and black arrows indicate AGO2 expression in acinar cells and islets of Langerhans, respectively. **c**, Representative H&E and IHC analysis for AGO2 in pancreata obtained from 12-week old mice from the *AGO2$^{+/+}$;KRAS^{G12D};p48Cre* and *AGO2$^{fl/fl}$;KRAS^{G12D};p48Cre* genotypes. Orange and black arrows indicate AGO2 staining in the PanIN and stromal regions, respectively. **d**, Scatter plot showing the weight of pancreata obtained from mice of the indicated genotypes aged over 400 days. **e**, Histogram showing

bioRxiv preprint doi: https://doi.org/10.1101/227264; this version posted November 30, 2017. The copyright holder for this preprint (which was not certified by peer review) is the author/funder, who has granted bioRxiv a license to display the preprint in perpetuity. It is made available under aCC-BY 4.0 International license.

average number of early and late PanIN lesions observed in 11 *KRAS^{G12D};p48Cre*, 11 *AGO2$^{fl/+}$;KRAS^{G12D};p48Cre* and 6 *AGO2$^{fl/fl}$;KRAS^{G12D};p48Cre* mice aged over 400 days. For *AGO2$^{fl/fl}$;KRAS^{G12D};p48Cre* mice, only lesions that do not express AGO2 have been included. **f**, Kaplan Meier curve for tumor-free survival of *KRAS^{G12D};p48Cre*, *AGO2$^{fl/+}$;KRAS^{G12D};p48Cre* and *AGO2$^{fl/fl}$; KRAS^{G12D};p48Cre* mice aged over 500 days. **g**, Chart showing PDAC (within the pancreas), the different metastatic lesions and abnormal pathologies (black boxes) observed in each mouse of the indicated genotypes aged over 500 days. Gray boxes in the *AGO2$^{fl/fl}$;KRAS^{G12D};p48Cre* group indicate abnormal pathology observed at the indicated site and is addressed further in detail in **Extended Data Figure 4**.

Figure 2 AGO2 protein expression increases at the plasma membrane during mouse and human PDAC progression. **a**, Representative images of AGO2 IHC analysis within an individual AGO2$^{+/+}$;*KRAS^{G12D}*;*p48Cre* mouse showing increased AGO2 expression in PDAC and metastasis compared to PanIN lesions. Arrows point to PanIN, PDAC, or metastatic PDAC in respective panels. In the metastasis panel, N=normal liver and T=tumor. Scale bar, 40µm. **b**, Representative images of IHC analysis for AGO2 expression in human PDAC progression showing elevated AGO2 protein expression in PDAC and metastatic tissue. Lower panels show higher magnifications of areas marked in the upper panels. Low and high magnification indicate 8X and 20X images, respectively. Arrows point to PanIN and PDAC. **c**, Box and scatter plot showing AGO2 expression on a human tissue microarray (TMA) containing 24 precancerous, 14 PDAC and 6 metastatic PDAC lesions, as determined by IHC analysis. Each sample was scored for intensity of stain and percent tumor cells staining for AGO2 and the final score = intensity x percent positive cells. p values were determined using t-test. **d**, Representative images of immunofluorescence analysis of human pancreatic tissue on a TMA showing co-localization of AGO2 and KRAS in PDAC cells. AGO2 and KRAS specific antibodies were used

bioRxiv preprint doi: https://doi.org/10.1101/227264; this version posted November 30, 2017. The copyright holder for this preprint (which was not certified by peer review) is the author/funder, who has granted bioRxiv a license to display the preprint in perpetuity. It is made available under aCC-BY 4.0 International license.

for the analyses and detected using Cy3 (green) and Cy5 (red) labeled secondary antibodies respectively. Arrows point to regions of overlap of red and green (yellow) signals indicative of co-localization. Scale bar, 100µm.

Figure 3 *AGO2* loss elevates phospho-EGFR levels to activate wild-type RAS. **a**, Immunoblot analysis of AGO2 and associated RAS signaling molecules from individual pancreata obtained from 12 week old mice of the indicated genotypes. **b,** Representative images of IHC analysis for pEGFR, EGFR and AGO2 in PanINs of 12 week old mice in the *KRAS^{G12D};p48Cre* and *AGO2$^{fl/fl}$;KRAS^{G12D};p48Cre* groups. **c**, Immunoblot analysis of EGFR-RAS signaling and RAS activation levels in pancreatic ductal organoids obtained from 12 week old *KRAS^{G12D};p48Cre* and *AGO2$^{fl/fl}$;KRAS^{G12D};p48Cre* mice. Organoids were cultured in the absence of EGF in culture medium for 9 weeks. Total RAS-GTP and fraction of KRASG12D-GTP levels were determined using the RAF binding assay followed by immunoblotting with KRASG12D specific or pan-RAS antibodies. **d**, Proliferation rates of pancreatic ductal organoids isolated from 12-week old mice from the indicated genotypes. Cell viability was measured using Cell Titer-Glo in the absence of EGF. Luminescence from five replicate wells per time point are represented. Error bars represent SEM. **e**, Immunoblot analysis of AGO2 and various EGFR-RAS signaling proteins in lysates of parental, *AGO2-/-* and *AGO2-/- + AGO2* mouse embryonic fibroblasts (MEF). RAS-GTP levels were determined by the RAF binding assay.

Figure 4 EGFR phosphorylation of AGO2^{Y393} disrupts wild-type KRAS-AGO2 interaction but not mutant KRAS-AGO2 interaction. **a**, Immunoprecipitation (IP) of endogenous AGO2 upon EGF stimulation (5'), in the indicated cancer cells expressing wild-type RAS followed by immunoblot analysis of KRAS. For MCF7 cells, endogenous co-IP analysis was performed

bioRxiv preprint doi: https://doi.org/10.1101/227264; this version posted November 30, 2017. The copyright holder for this preprint (which was not certified by peer review) is the author/funder, who has granted bioRxiv a license to display the preprint in perpetuity. It is made available under aCC-BY 4.0 International license.

using both AGO2 and KRAS specific antibodies. For each cell line, MAPK activation and levels of various proteins are shown as input blots. **b,** IP of endogenous AGO2 upon EGF stimulation (5'), in the indicated cancer cells harboring different *KRAS* mutations, followed by immunoblot analysis of KRAS. For each cell line, MAPK activation and levels of various proteins are shown as input blots. Co-IP and immunoblot analysis of RAS and AGO2 upon EGF stimulation of HEK293 ($KRAS^{WT}$) cells expressing FLAG-AGO2 **c**, or DLD-1 ($KRAS^{G13D}$) **d**, cells in the presence or absence of erlotinib. Input blots show MAPK activation and levels of indicated proteins. EGF stimulation and RAS co-IP analysis in HEK293 ($KRAS^{WT}$) **e**, or MIA-PaCa-2 ($KRAS^{G12C}$) **f**, cells expressing FLAG-tagged *AGO2* (WT or Y393F). Immunoblot analysis for AGO2 binding was performed using FLAG antibodies. For each cell line, input blots show MAPK activation and the relative levels of indicated proteins. **g**, Schematic showing the regulation of wild-type KRAS-AGO2 interaction upon EGFR activation. By contrast, mutant KRAS is recalcitrant to regulation by EGFR and remains associated with AGO2.

Acknowledgements

We thank Mandy Davis and Marta Hernadi-Muller for their help with processing paraffin embedded slides. We also thank Malay Mody and Markus Eberl for technical assistance and Eric Fearon for discussion. A.M.C is an American Cancer Society Research Professor and Taubman Scholar.

Conflict of Interest

The authors have no conflict of interests related to this study.

Author Contributions

Mouse experimental data was generated by J.C.T, S.S., K.M.J, A.W, A.G, and G.T. Contributions to other experimental data were made by S.S., R.F.S, V.L.D, S.Z-W, M.M, J.S.,

bioRxiv preprint doi: https://doi.org/10.1101/227264; this version posted November 30, 2017. The copyright holder for this preprint (which was not certified by peer review) is the author/funder, who has granted bioRxiv a license to display the preprint in perpetuity. It is made available under aCC-BY 4.0 International license.

I.J.A. and C.K-S. L.W. and J.S. did pathology assessment, J.S. provided the human TMA and performed IHC scoring. S.S. and A.M.C. jointly conceived the study. S.S., C.K-S. and A.M.C. wrote the manuscript. Funding and overall supervision of the study was provided by A.M.C.

Methods

Mouse strains

LSL-*KRASG12D*[7] (Kras $^{LSL\text{-}G12D/+}$) and p48Cre[44] (*Ptf1a-Cre* or *Ptf1a*$^{Cre/+}$) mice were obtained from Marina Pasca di Magliano, University of Michigan. Conditionally floxed *AGO2*[13] (*AGO2*$^{fl/fl}$) mice were purchased from Jackson labs (Bar Harbor, Maine). PCR genotyping for *KRAS*^{G12D}, *p48Cre* and *AGO2* alleles, from DNA isolated from mouse tails, was performed using standard methodology. To generate experimental and control mice, *AGO2*$^{fl/fl}$, *p48Cre*, and *KRAS*^{G12D} lines were intercrossed to generate *AGO2*$^{fl/+}$;*p48Cre* and *KRAS*^{G12D}; p48Cre mice. These two lines were then intercrossed to generate the *AGO2*$^{fl/fl}$;*KRAS*^{G12D};*p48Cre* experimental mice. Given that mice were maintained on a mixed background; littermate controls were systematically used in all experiments (sex ratio per cohort was balanced). All animals were housed in a pathogen-free environment, and all procedures were performed in accordance with requirements of the University of Michigan IACUC.

Cre activation in acinar cells of pancreata of mice with mutant KRAS alleles was validated by genotyping using the *KRAS*^{G12D} conditional PCR primers 5' *gtc ttt ccc cag cac agt gc* 3', 5' *ctc ttg cct acg cca cca gct c* 3' and 5' *agc tag cca cca tgg ctt gag taa gtc tgc a* 3' according to Tyler Jacks lab protocol (https://jacks-lab.mit.edu/protocols/genotyping/kras_cond).

Histology, immunohistochemistry and immunofluorescence

Paraffin embedded tissues from mice were processed using standard methodology. Details of the primary antibodies used for IHC are provided in **Extended Data Table 1**. For

bioRxiv preprint doi: https://doi.org/10.1101/227264; this version posted November 30, 2017. The copyright holder for this preprint (which was not certified by peer review) is the author/funder, who has granted bioRxiv a license to display the preprint in perpetuity. It is made available under aCC-BY 4.0 International license.

immunofluorescence analysis, Alexa Fluor Cyanine Cy3 Anti-Rabbit (1:200) and Cy5 Anti-Mouse (1:200) (Jackson Immunoresearch) were used as secondary antibodies.

Human TMA analysis

Pancreatic TMAs were developed at the Tissue and Molecular Pathology Core at the Department of Pathology, University of Michigan after IRB approval. IHC scoring was performed by a pathologist.

Quantitative microRNA and mRNA RT-PCR

Pancreatic total RNA was isolated using AllPrep DNA/RNA/miRNA Universal Kit (Qiagen). 5ng of total RNA from each sample was converted into cDNA using miRCURY™ LNA™ Universal RT microRNA PCR Universal cDNA Synthesis Kit II. Quantitative micro RT-PCR was performed using exiLENT SYBR Green master mix with microRNA ready to use PCR mix, Mouse&Rat panel I, V4.M (Exiqon , Cat # 203713) on ABI 7900HT Fast Real time PCR system(Applied Biosystems). Data was analysed using GenEX ver 6 software.

For quantitation of mRNA transcripts, RNA was extracted from the indicated samples and cDNA was synthesized using SuperScript III System according to the manufacturer's instructions (Invitrogen). Quantitative RT-PCR was conducted using primers detailed in **Extended Data Table 3** with SYBR Green Master Mix (Applied Biosystems) on the StepOne Real-Time PCR System (Applied Biosystems). Relative mRNA levels of the transcripts were normalized to the expression of the housekeeping gene *GAPDH*.

Pancreatic tissue lysates and immunoblot analysis

Pancreata obtained from mice were homogenized in Mg^{2+} containing lysis buffer. Clear lysates were separated using SDS-PAGE and processed for immunoblot analysis using standard methods. Primary antibodies used in the study are indicated in **Extended Data Table 1**. Particularly, Ras antibodies validated in a recent study[45] are also indicated.

Isolation of pancreatic ductal organoids

bioRxiv preprint doi: https://doi.org/10.1101/227264; this version posted November 30, 2017. The copyright holder for this preprint (which was not certified by peer review) is the author/funder, who has granted bioRxiv a license to display the preprint in perpetuity. It is made available under aCC-BY 4.0 International license.

Pancreatic ductal organoids obtained from 12 week old *KRAS^{G12D};p48Cre* and *AGO2$^{fl/fl}$;KRAS^{G12D};p48Cre* mice were cultured in organoid media as described previously[26]. Organoids were cultured without EGF for (17 passages) 9 weeks to exclude normal duct contamination which are dependent on EGF. Ductal organoid proliferation assay was performed using Cell Titer-Glo (Promega).

RAS-GTP analysis

Protein lysates were prepared from pancreatic ductal organoids or cell lines using Mg^{2+} containing lysis buffer. RAF1 binding was used as a measure of RAS-GTP levels in the lysates as shown before[5].

Plasmids

Full length FH-*AGO2* constructs were obtained from Addgene (pIRESneo-FLAG/HA-AGO2 10822, PI:Thomas Tuschl). *AGO2Y393F* mutant construct was generated using the QuikChange II XL Site-Directed Mutagenesis Kit (Agilent) from the FH-*AGO2* plasmid described above using the primers hAGO2_Y393F_Fwd 5'*AAATTCACGGACGAATGGATCTGTGTTGAAACTTGCAC*3' and hAGO2_Y393F_Rev 5'*GTGCAAGTTTCAACACAGATCCATTCGTCCGTGAATTT*3'. DNA sequence were confirmed using Sanger sequencing at the University of Michigan Sequencing Core.

Cell culture, transfection and EGF stimulation

All cell lines (detailed in **Extended Data Table 4**) were obtained from the American Type Culture Collection (ATCC). Cells were cultured following ATCC culture methods in media supplemented with the corresponding serum and antibiotics. Additionally, cells were routinely genotyped and tested bi-weekly for mycoplasma contamination. For EGF stimulation, cells were grown to approximately 80% confluence and washed with PBS three times. Cells were incubated overnight (16 hr) in serum free media. EGF stimulation was performed for 5 minutes

bioRxiv preprint doi: https://doi.org/10.1101/227264; this version posted November 30, 2017. The copyright holder for this preprint (which was not certified by peer review) is the author/funder, who has granted bioRxiv a license to display the preprint in perpetuity. It is made available under aCC-BY 4.0 International license.

with 100 ng/ul of epidermal growth factor (Gibco) at 37°C. After stimulation, cells were washed and protein lysates were prepared in K Buffer lysis buffer. For tyrosine kinase inhibition, cells were pretreated with 15 uM of Erlotinib for 1 hour prior to EGF stimulation, as described above.

HEK293 or MIA PaCa-2 cells were transfected with different *AGO2* constructs using Fugene HD (Promega) or Lipofectamine 3000 (Invitrogen) according to the manufacturer's protocols. For EGFR stimulation with transient AGO2 construct overexpression, cells were transfected approximately 16 hours prior to overnight serum starvation and EGF stimulation.

Immunoprecipitation (IP) Analysis

For immunoprecipitation analysis protein lysates were prepared in K Buffer (20mM Tris pH 7.0, 5 mM EDTA, 150mM NaCl, 1% Triton X100, 1 mM DTT, phosphatase inhibitors, and protease inhibitors). Typically,150-200 ug of protein lysates (RAS10 IP: 150 ug; AGO2 IP: 200 ug; KRAS IP: 150 ug) were pre-cleared with 10 ul of Protein A/G agarose beads (Santa Cruz) for 1 hour. Pre-cleared lysates were incubated with 5-10 ug of the indicated primary antibodies targeting protein of interest or with corresponding isotype controls overnight at 4°C. 30 ul of Protein A/G beads were then added to immune complexes and incubated for 1-3 hours at 4°C, spun, washed in 150-300 mM NaCl containing K-buffer prior to separation of immunoprecipitates by SDS PAGE. To determine the varying levels of KRAS expressed in different cells lines (with or without EGF stimulation), shown in **Fig. 4**., pan RAS10 antibody was used for immunoprecipitation followed by immunoblot analysis using KRAS specific SC-30 antibody.

RAS-GTP pull down assay

The RAS-RAF interaction was studied using the RBD agarose beads as per manufacturer's instructions (Millipore). Pull down assays were performed using the lysates from pancreatic ductal organoids and cell lines as indicated. The pull down of RAS by RBD agarose beads indicates the presence of active GTP-bound RAS interacting with RAF1.

bioRxiv preprint doi: https://doi.org/10.1101/227264; this version posted November 30, 2017. The copyright holder for this preprint (which was not certified by peer review) is the author/funder, who has granted bioRxiv a license to display the preprint in perpetuity. It is made available under aCC-BY 4.0 International license.

References

1. Almoguera, C., *et al.* Most human carcinomas of the exocrine pancreas contain mutant c-K-ras genes. *Cell* **53**, 549-554 (1988).
2. Chin, L., *et al.* Essential role for oncogenic Ras in tumour maintenance. *Nature* **400**, 468-472 (1999).
3. Ardito, C.M., *et al.* EGF receptor is required for KRAS-induced pancreatic tumorigenesis. *Cancer Cell* **22**, 304-317 (2012).
4. Navas, C., *et al.* EGF receptor signaling is essential for k-ras oncogene-driven pancreatic ductal adenocarcinoma. *Cancer Cell* **22**, 318-330 (2012).
5. Shankar, S., *et al.* KRAS Engages AGO2 to Enhance Cellular Transformation. *Cell Rep* **14**, 1448-1461 (2016).
6. Shen, J., *et al.* EGFR modulates microRNA maturation in response to hypoxia through phosphorylation of AGO2. *Nature* **497**, 383-387 (2013).
7. Hingorani, S.R., *et al.* Preinvasive and invasive ductal pancreatic cancer and its early detection in the mouse. *Cancer Cell* **4**, 437-450 (2003).
8. Guerra, C. & Barbacid, M. Genetically engineered mouse models of pancreatic adenocarcinoma. *Mol Oncol* **7**, 232-247 (2013).
9. Kleeff, J., *et al.* Pancreatic cancer. *Nat Rev Dis Primers* **2**, 16022 (2016).
10. Rajalingam, K., Schreck, R., Rapp, U.R. & Albert, S. Ras oncogenes and their downstream targets. *Biochim Biophys Acta* **1773**, 1177-1195 (2007).
11. Pylayeva-Gupta, Y., Grabocka, E. & Bar-Sagi, D. RAS oncogenes: weaving a tumorigenic web. *Nat Rev Cancer* **11**, 761-774 (2011).
12. Simanshu, D.K., Nissley, D.V. & McCormick, F. RAS Proteins and Their Regulators in Human Disease. *Cell* **170**, 17-33 (2017).
13. O'Carroll, D., *et al.* A Slicer-independent role for Argonaute 2 in hematopoiesis and the microRNA pathway. *Genes Dev* **21**, 1999-2004 (2007).
14. Kopp, J.L., *et al.* Identification of Sox9-dependent acinar-to-ductal reprogramming as the principal mechanism for initiation of pancreatic ductal adenocarcinoma. *Cancer Cell* **22**, 737-750 (2012).
15. Qiu, W., *et al.* Disruption of p16 and activation of Kras in pancreas increase ductal adenocarcinoma formation and metastasis in vivo. *Oncotarget* **2**, 862-873 (2011).
16. Morris, J.P.t., *et al.* Dicer regulates differentiation and viability during mouse pancreatic cancer initiation. *PLoS One* **9**, e95486 (2014).
17. Hingorani, S.R., *et al.* Trp53R172H and KrasG12D cooperate to promote chromosomal instability and widely metastatic pancreatic ductal adenocarcinoma in mice. *Cancer Cell* **7**, 469-483 (2005).
18. Herreros-Villanueva, M., Hijona, E., Cosme, A. & Bujanda, L. Mouse models of pancreatic cancer. *World J Gastroenterol* **18**, 1286-1294 (2012).
19. Collins, M.A., *et al.* Metastatic pancreatic cancer is dependent on oncogenic Kras in mice. *PLoS One* **7**, e49707 (2012).
20. Schmick, M., *et al.* KRas localizes to the plasma membrane by spatial cycles of solubilization, trapping and vesicular transport. *Cell* **157**, 459-471 (2014).

bioRxiv preprint doi: https://doi.org/10.1101/227264; this version posted November 30, 2017. The copyright holder for this preprint (which was not certified by peer review) is the author/funder, who has granted bioRxiv a license to display the preprint in perpetuity. It is made available under aCC-BY 4.0 International license.

21. Johnson, S.M., *et al.* RAS is regulated by the let-7 microRNA family. *Cell* **120**, 635-647 (2005).
22. Ravi, A., *et al.* Proliferation and tumorigenesis of a murine sarcoma cell line in the absence of DICER1. *Cancer Cell* **21**, 848-855 (2012).
23. Liu, J., *et al.* Argonaute2 is the catalytic engine of mammalian RNAi. *Science* **305**, 1437-1441 (2004).
24. Faehnle, C.R., Elkayam, E., Haase, A.D., Hannon, G.J. & Joshua-Tor, L. The making of a slicer: activation of human Argonaute-1. *Cell Rep* **3**, 1901-1909 (2013).
25. Siveke, J.T. & Crawford, H.C. KRAS above and beyond - EGFR in pancreatic cancer. *Oncotarget* **3**, 1262-1263 (2012).
26. Boj, S.F., *et al.* Organoid models of human and mouse ductal pancreatic cancer. *Cell* **160**, 324-338 (2015).
27. Zhang, Z., *et al.* Wildtype Kras2 can inhibit lung carcinogenesis in mice. *Nat Genet* **29**, 25-33 (2001).
28. Zhou, B., Der, C.J. & Cox, A.D. The role of wild type RAS isoforms in cancer. *Semin Cell Dev Biol* **58**, 60-69 (2016).
29. Broderick, J.A., Salomon, W.E., Ryder, S.P., Aronin, N. & Zamore, P.D. Argonaute protein identity and pairing geometry determine cooperativity in mammalian RNA silencing. *RNA* **17**, 1858-1869 (2011).
30. Oda, K., Matsuoka, Y., Funahashi, A. & Kitano, H. A comprehensive pathway map of epidermal growth factor receptor signaling. *Mol Syst Biol* **1**(2005).
31. Lowenstein, E.J., *et al.* The Sh2 and Sh3 Domain Containing Protein Grb2 Links Receptor Tyrosine Kinases to Ras Signaling. *Cell* **70**, 431-442 (1992).
32. Hayes, T.K. & Der, C.J. Mutant and Wild-type Ras: Co-conspirators in Cancer. *Cancer Discov* **3**, 24-26 (2013).
33. Young, A., Lou, D. & McCormick, F. Oncogenic and Wild-type Ras Play Divergent Roles in the Regulation of Mitogen-Activated Protein Kinase Signaling. *Cancer Discov* **3**, 112-123 (2013).
34. Perez-Mancera, P.A., Guerra, C., Barbacid, M. & Tuveson, D.A. What we have learned about pancreatic cancer from mouse models. *Gastroenterology* **142**, 1079-1092 (2012).
35. Gutmann, D.H., Hunter-Schaedle, K. & Shannon, K.M. Harnessing preclinical mouse models to inform human clinical cancer trials. *J Clin Invest* **116**, 847-852 (2006).
36. Mazur, P.K., *et al.* Notch2 is required for progression of pancreatic intraepithelial neoplasia and development of pancreatic ductal adenocarcinoma. *Proc Natl Acad Sci U S A* **107**, 13438-13443 (2010).
37. Krol, J., Loedige, I. & Filipowicz, W. The widespread regulation of microRNA biogenesis, function and decay. *Nat Rev Genet* **11**, 597-610 (2010).
38. Johnson, S.M., *et al.* RAS is regulated by the let-7 microRNA family. *Cell* **120**, 635-647 (2005).
39. Wee, P. & Wang, Z.X. Epidermal Growth Factor Receptor Cell Proliferation Signaling Pathways. *Cancers* **9**(2017).
40. Lehr, S., *et al.* Identification of tyrosine phosphorylation sites in human Gab-1 protein by EGF receptor kinase in vitro. *Biochemistry* **38**, 151-159 (1999).
41. Furcht, C.M., Buonato, J.M. & Lazzara, M.J. EGFR-activated Src family kinases maintain GAB1-SHP2 complexes distal from EGFR. *Sci Signal* **8**, ra46 (2015).
42. Li, S., Couvillon, A.D., Brasher, B.B. & Van Etten, R.A. Tyrosine phosphorylation of Grb2 by Bcr/Abl and epidermal growth factor receptor: a novel regulatory mechanism for tyrosine kinase signaling. *EMBO J* **20**, 6793-6804 (2001).
43. Karnoub, A.E. & Weinberg, R.A. Ras oncogenes: split personalities. *Nat Rev Mol Cell Biol* **9**, 517-531 (2008).

bioRxiv preprint doi: https://doi.org/10.1101/227264; this version posted November 30, 2017. The copyright holder for this preprint (which was not certified by peer review) is the author/funder, who has granted bioRxiv a license to display the preprint in perpetuity. It is made available under aCC-BY 4.0 International license.

44. Kawaguchi, Y., *et al.* The role of the transcriptional regulator Ptf1a in converting intestinal to pancreatic progenitors. *Nat Genet* **32**, 128-134 (2002).
45. Waters, A.M., *et al.* Evaluation of the selectivity and sensitivity of isoform- and mutation-specific RAS antibodies. *Sci Signal* **10**(2017).

Figure 1

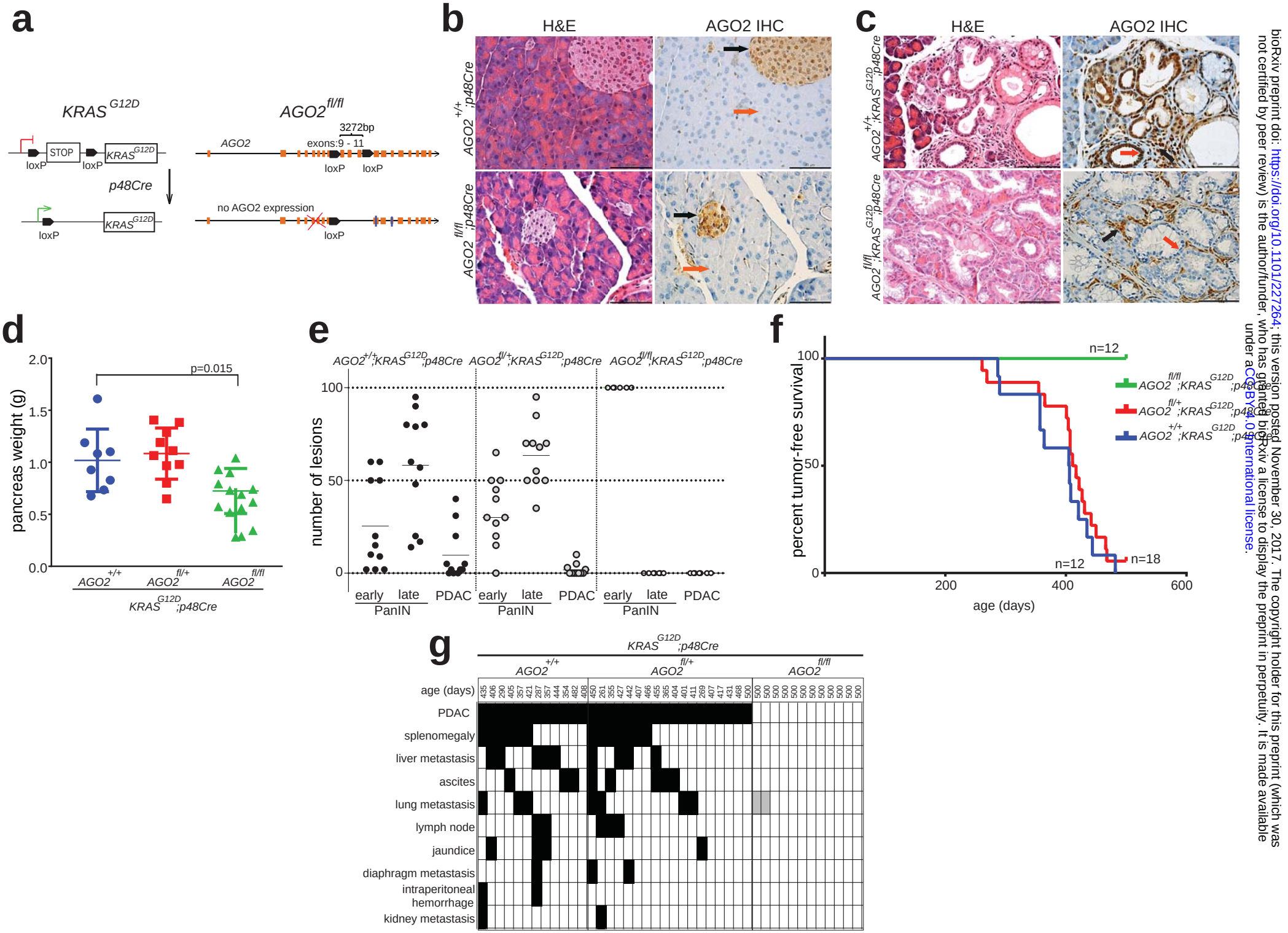

bioRxiv preprint doi: https://doi.org/10.1101/227264; this version posted November 30, 2017. The copyright holder for this preprint (which was not certified by peer review) is the author/funder, who has granted bioRxiv a license to display the preprint in perpetuity. It is made available under aCC BY 4.0 International license.

bioRxiv preprint doi: https://doi.org/10.1101/227264; this version posted November 30, 2017. The copyright holder for this preprint (which was not certified by peer review) is the author/funder, who has granted bioRxiv a license to display the preprint in perpetuity. It is made available under aCC-BY 4.0 International license.

Figure 2

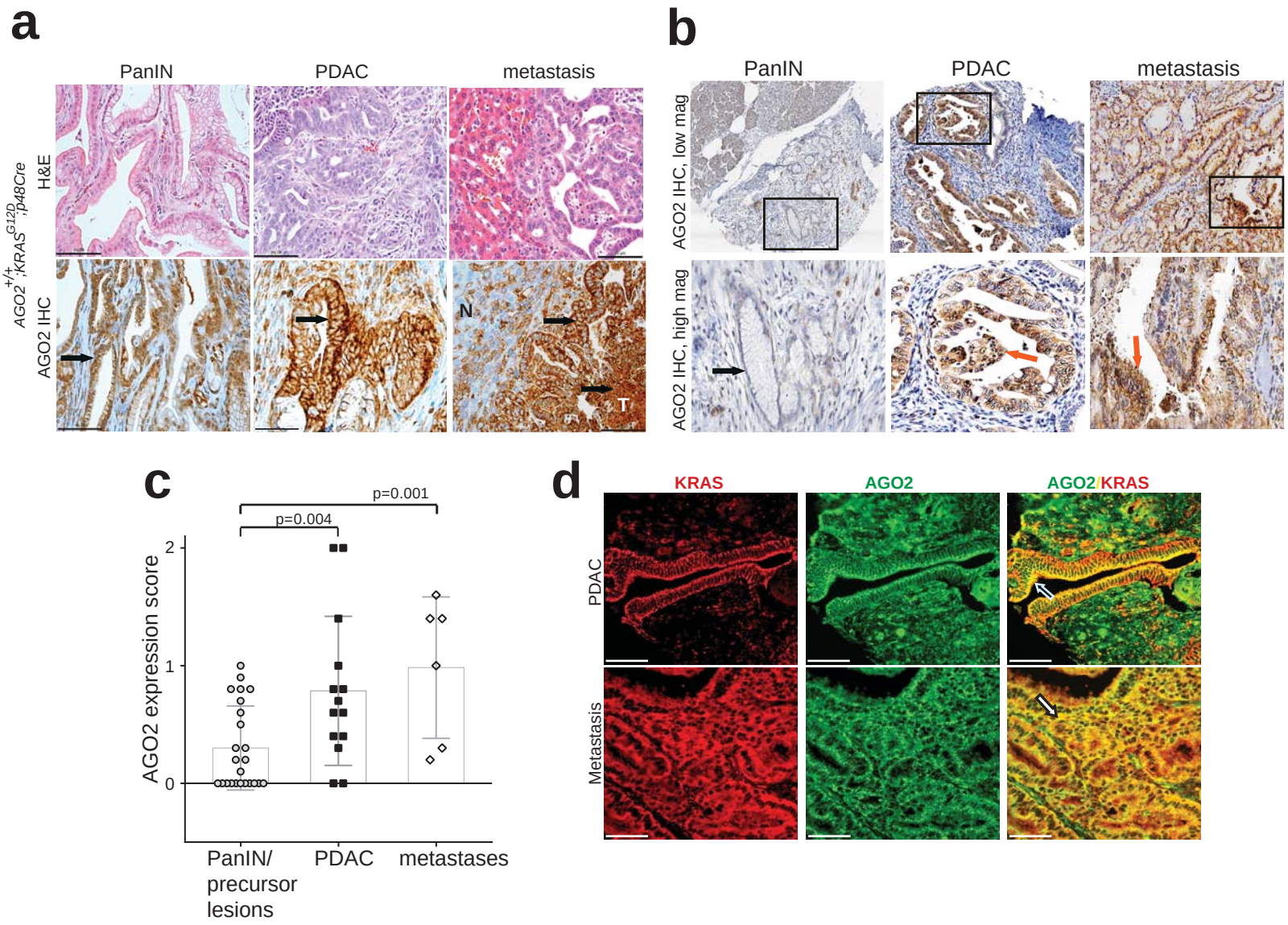

bioRxiv preprint doi: https://doi.org/10.1101/227264; this version posted November 30, 2017. The copyright holder for this preprint (which was not certified by peer review) is the author/funder, who has granted bioRxiv a license to display the preprint in perpetuity. It is made available under aCC-BY 4.0 International license.

Figure 3

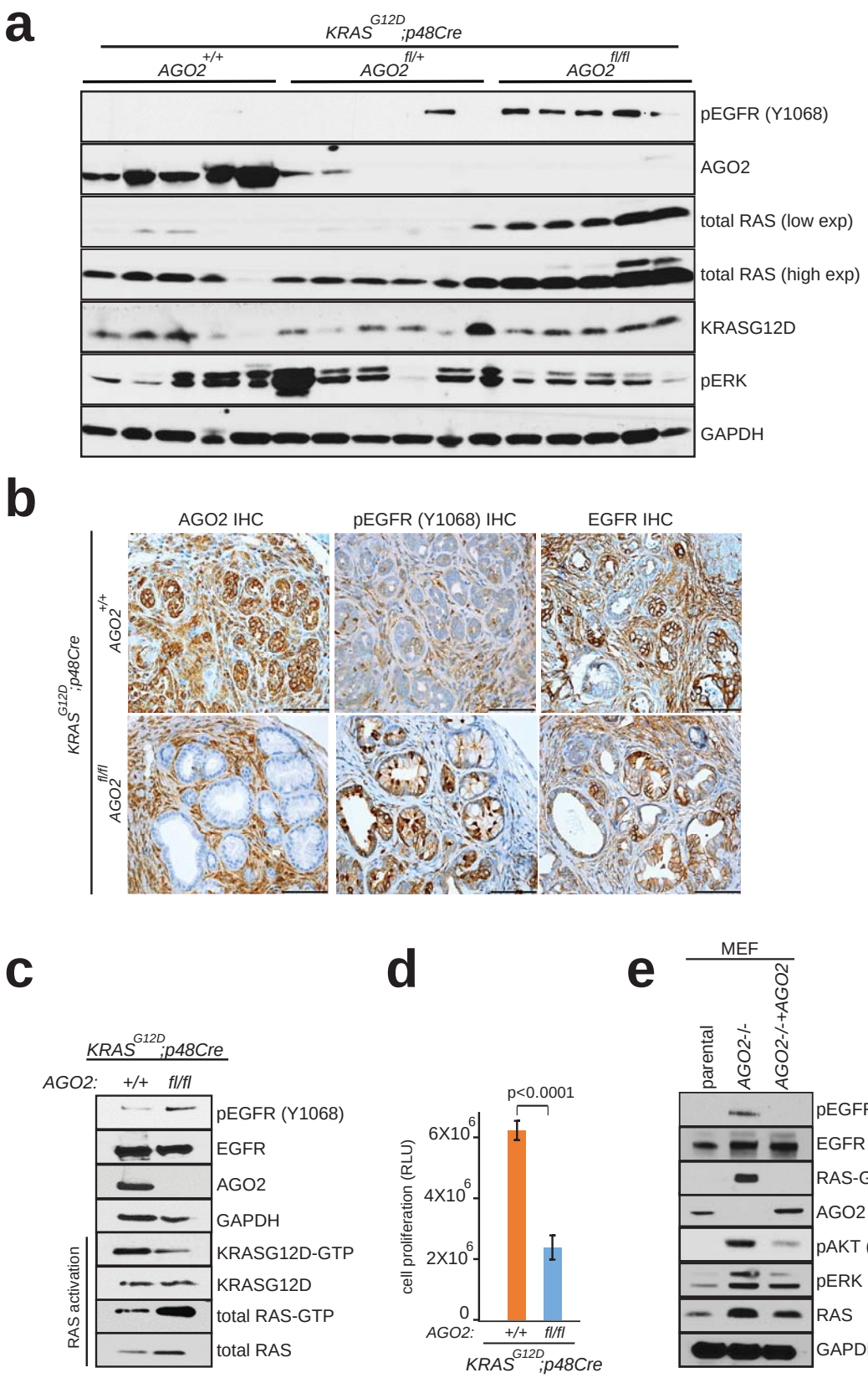

bioRxiv preprint doi: https://doi.org/10.1101/227264; this version posted November 30, 2017. The copyright holder for this preprint (which was not certified by peer review) is the author/funder, who has granted bioRxiv a license to display the preprint in perpetuity. It is made available under aCC-BY 4.0 International license.

Figure 4

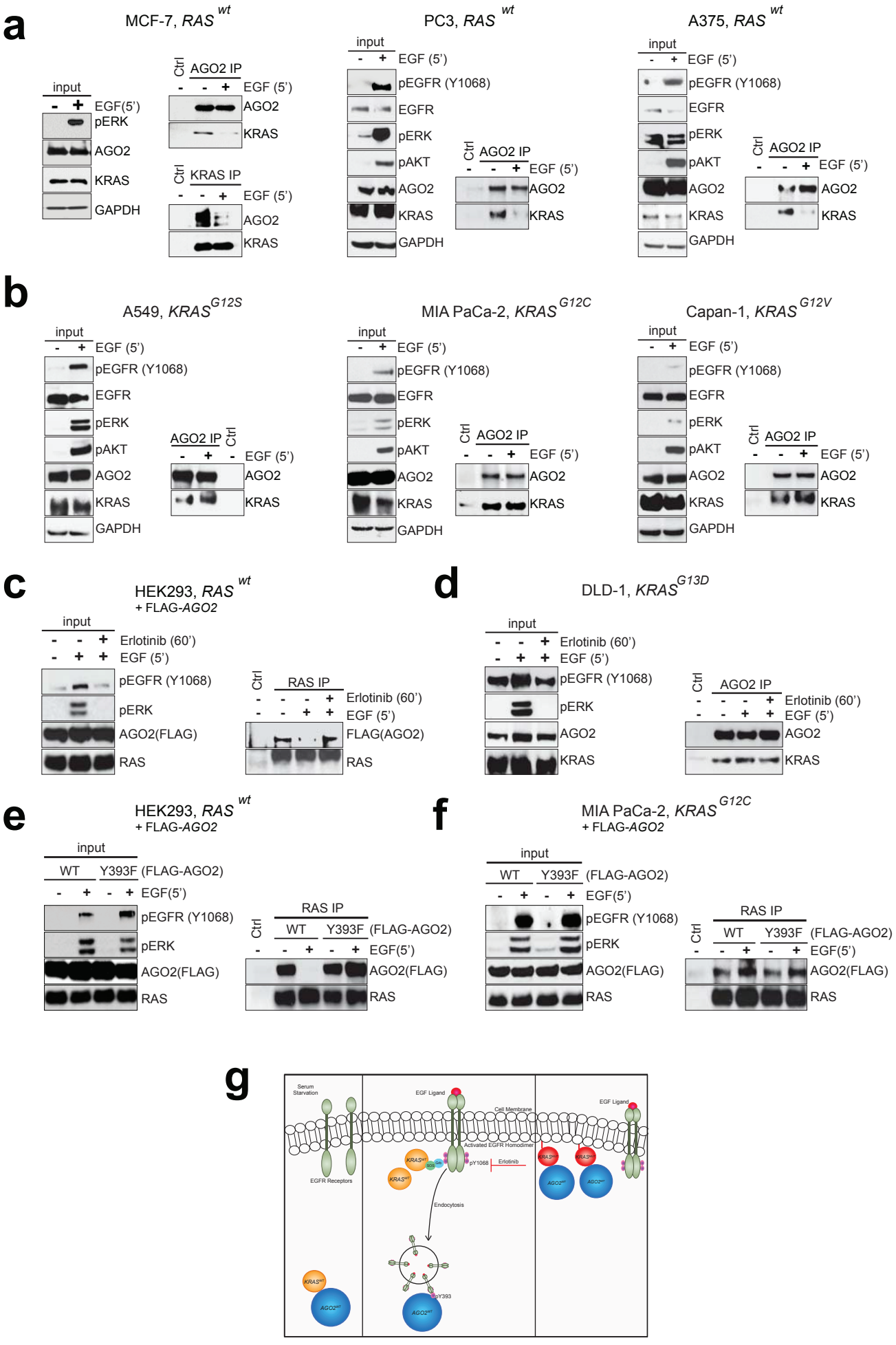

bioRxiv preprint doi: https://doi.org/10.1101/227264; this version posted November 30, 2017. The copyright holder for this preprint (which was not certified by peer review) is the author/funder, who has granted bioRxiv a license to display the preprint in perpetuity. It is made available under aCC-BY 4.0 International license.

Extended Data Figure 1

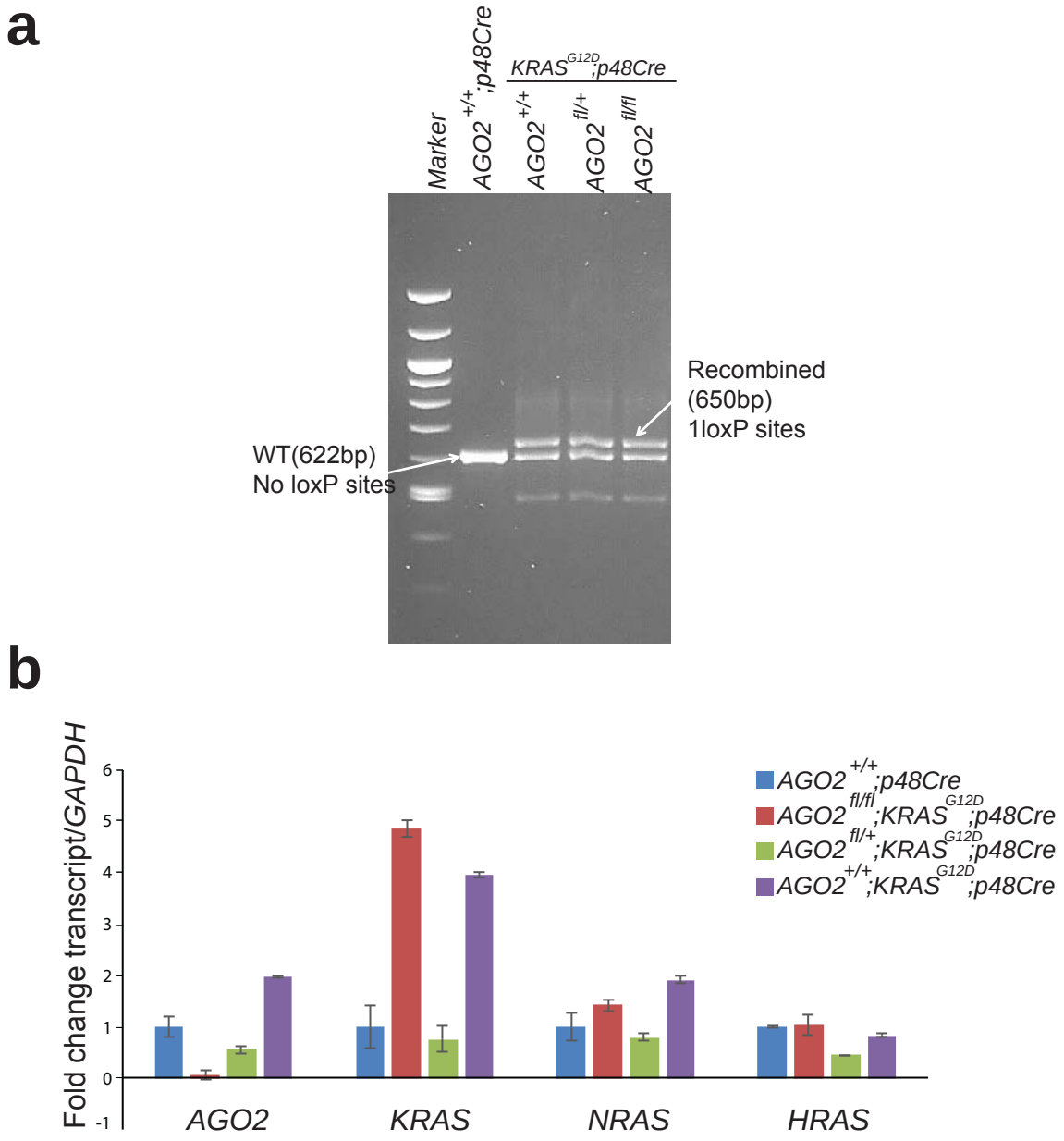

Extended Data Figure 1: Validation of Cre activation in the mouse model. (**a**) Genomic DNA analysis from the pancreata of the indicated genotypes showing recombined alleles in the LSL-*KRAS* model as described earlier(1) (**b**) RT-qPCR analysis for different transcripts from 10 week old mouse pancreata of the indicated genotypes.

bioRxiv preprint doi: https://doi.org/10.1101/227264; this version posted November 30, 2017. The copyright holder for this preprint (which was not certified by peer review) is the author/funder, who has granted bioRxiv a license to display the preprint in perpetuity. It is made available under aCC-BY 4.0 International license.

Extended Data Figure 2

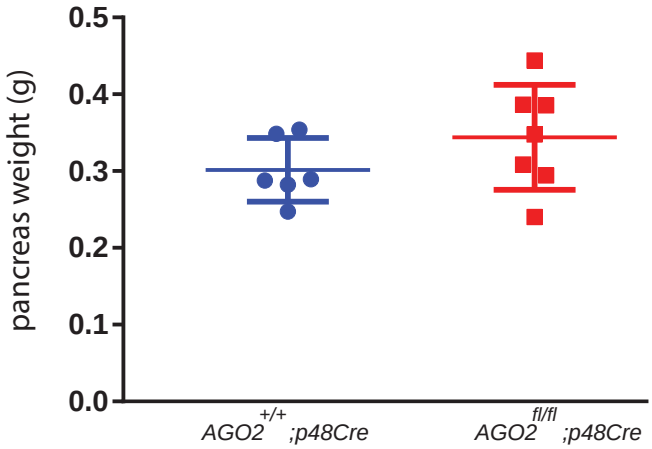

Extended Data Figure 2: Weight of pancreata obtained from 12 week old *AGO2*$^{+/+}$*;p48Cre* and *AGO2*$^{fl/fl}$*;p48Cre* mice.

bioRxiv preprint doi: https://doi.org/10.1101/227264; this version posted November 30, 2017. The copyright holder for this preprint (which was not certified by peer review) is the author/funder, who has granted bioRxiv a license to display the preprint in perpetuity. It is made available under aCC-BY 4.0 International License.

Extended Data Figure 3

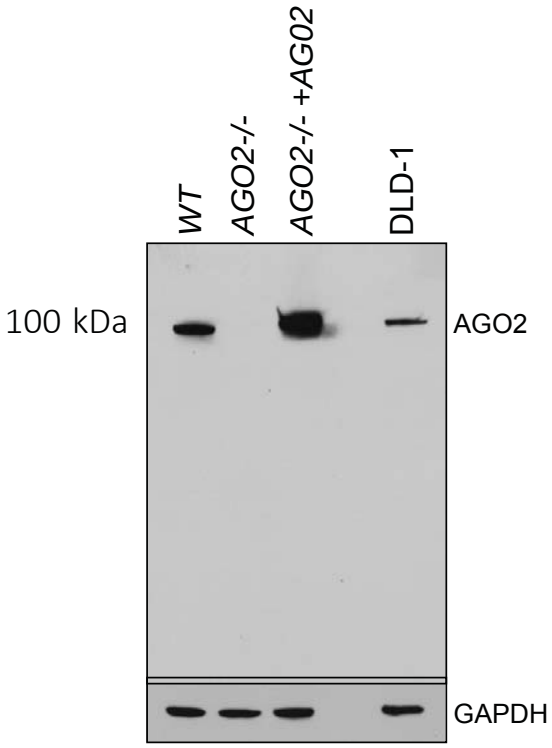

Extended Data Figure 3: Western blot analysis of AGO2-/- mouse embryonic fibroblasts and human colon cancer cells using a monoclonal antibody to AGO2 to confirm specificity of the antibody prior to use in immunohistochemistry (IHC). Further details are provided in Table 1.

bioRxiv preprint doi: https://doi.org/10.1101/227264; this version posted November 30, 2017. The copyright holder for this preprint (which was not certified by peer review) is the author/funder, who has granted bioRxiv a license to display the preprint in perpetuity. It is made available under aCC-BY 4.0 International license.

Extended Data Figure 4

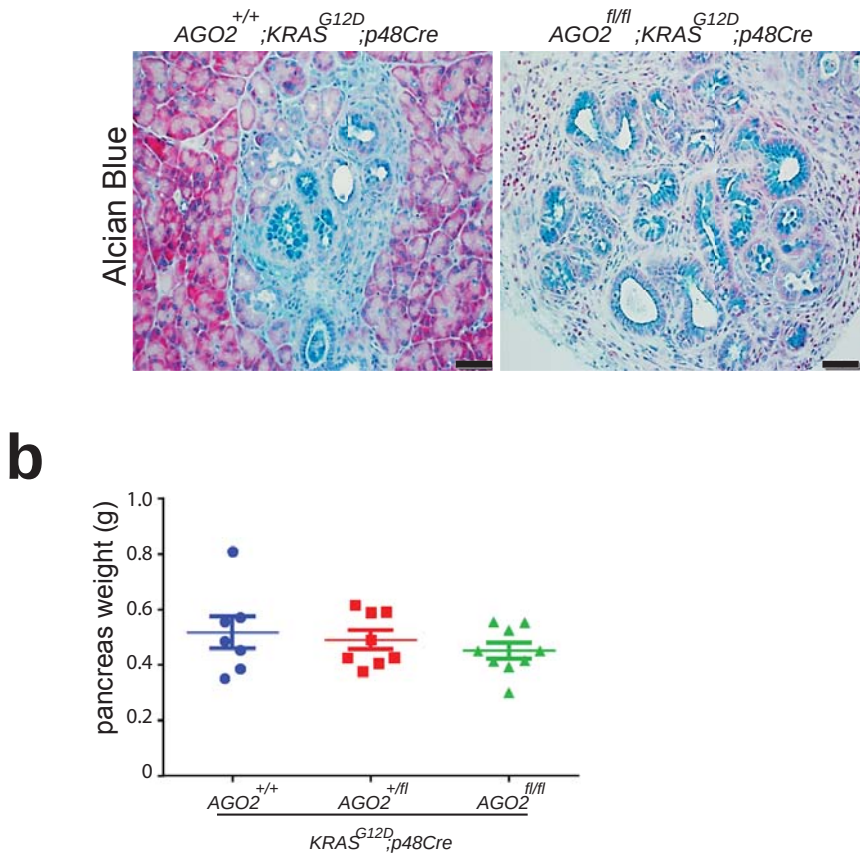

Extended Data Figure 4: PanINs observed in *AGO2$^{+/+}$;KRAS^{G12D};p48Cre* and *AGO2$^{fl/fl}$;KRAS^{G12D};p48Cre* are similar. **a**. Alcian Blue (mucin) staining of PanINs of the indicated genotypes **b**. Scatter plot showing the weight of pancreata obtained from mice of three indicated genotypes at 12 weeks of age.

bioRxiv preprint doi: https://doi.org/10.1101/227264; this version posted November 30, 2017. The copyright holder for this preprint (which was not certified by peer review) is the author/funder, who has granted bioRxiv a license to display the preprint in perpetuity. It is made available under aCC-BY 4.0 International License.

Extended Data Figure 5

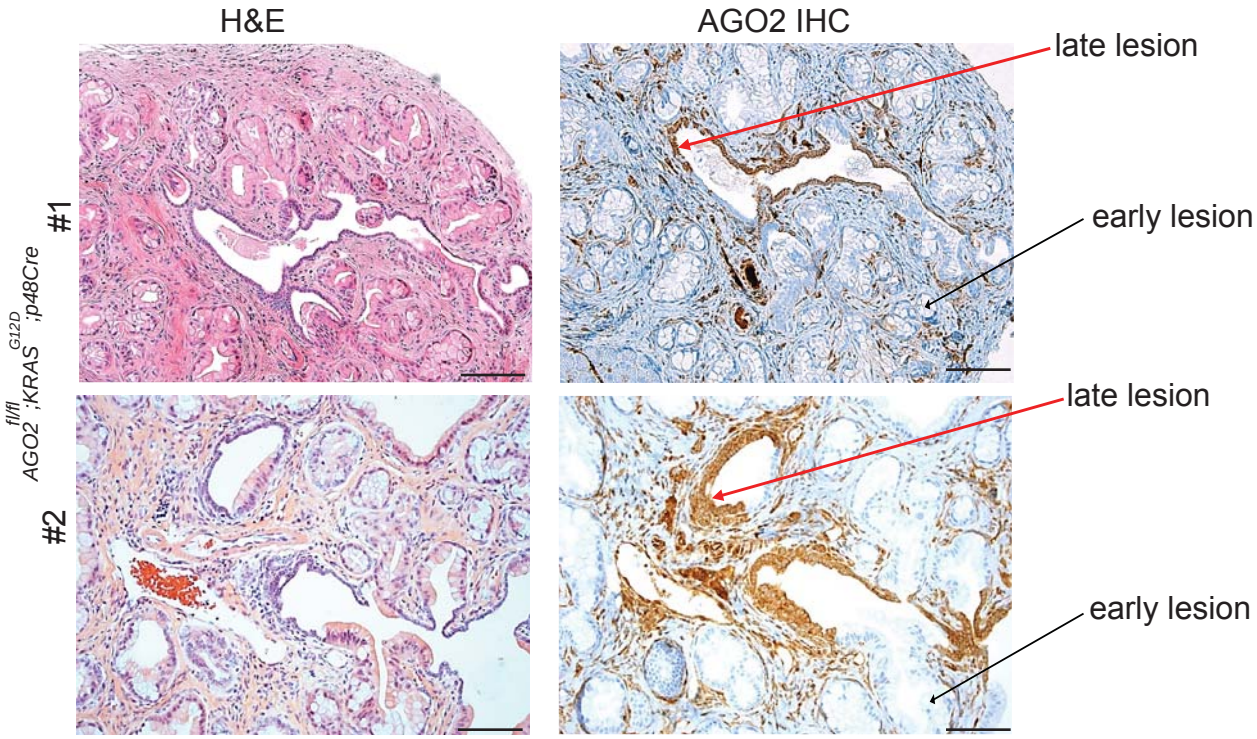

Extended Data Figure 5: Representative images of H&E and AGO2 IHC from two animals of the *AGO2*$^{fl/fl}$*;KRAS*^{G12D}*;p48Cre* cohort showing AGO2 expression in the late lesions. Scale bar represents 100μm and 40μm for upper and lower panels respectively.

bioRxiv preprint doi: https://doi.org/10.1101/227264; this version posted November 30, 2017. The copyright holder for this preprint (which was not certified by peer review) is the author/funder, who has granted bioRxiv a license to display the preprint in perpetuity. It is made available under aCC-BY 4.0 International license.

Extended Data Figure 6

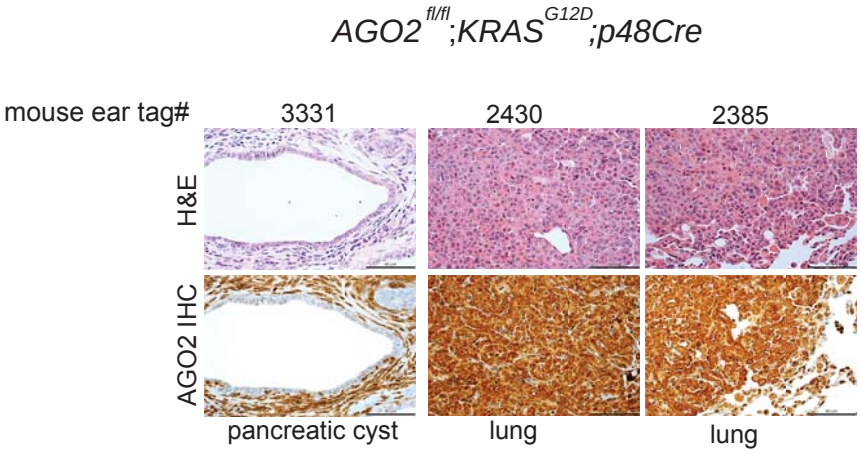

Extended Data Figure 6: H&E and AGO2 IHC analysis of abnormal pancreas and lungs from the *AGO2$^{fl/fl}$;KRAS^{G12D};p48Cre* mouse cohort (further detailed in Table 2). Scale bar, 100μm.

bioRxiv preprint doi: https://doi.org/10.1101/227264; this version posted November 30, 2017. The copyright holder for this preprint (which was not certified by peer review) is the author/funder, who has granted bioRxiv a license to display the preprint in perpetuity. It is made available under aCC-BY 4.0 International license.

Extended Data Figure 7

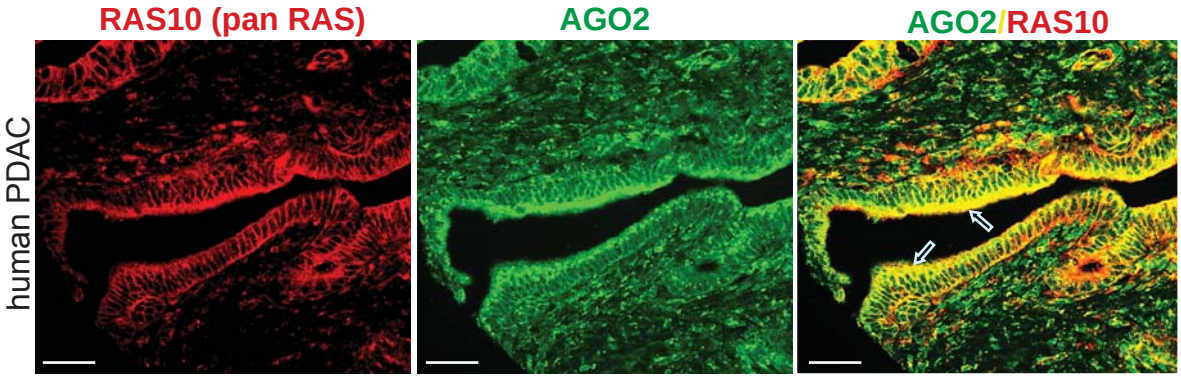

Extended Data Figure 7: Representative images of immunofluorescence analysis of human pancreatic tissue on a TMA showing co-localization of AGO2 and RAS in PDAC cells. AGO2 and pan RAS (RAS10) antibodies were used for the analyses and detected using Cy3 (green) and Cy5 (red) labeled secondary antibodies respectively. Arrows point to regions of overlap of red and green (yellow) signals indicative of co-localization. Scale bar, 100μm.

bioRxiv preprint doi: https://doi.org/10.1101/227264; this version posted November 30, 2017. The copyright holder for this preprint (which was not certified by peer review) is the author/funder, who has granted bioRxiv a license to display the preprint in perpetuity. It is made available under aCC-BY 4.0 International license.

Extended Data Figure 8

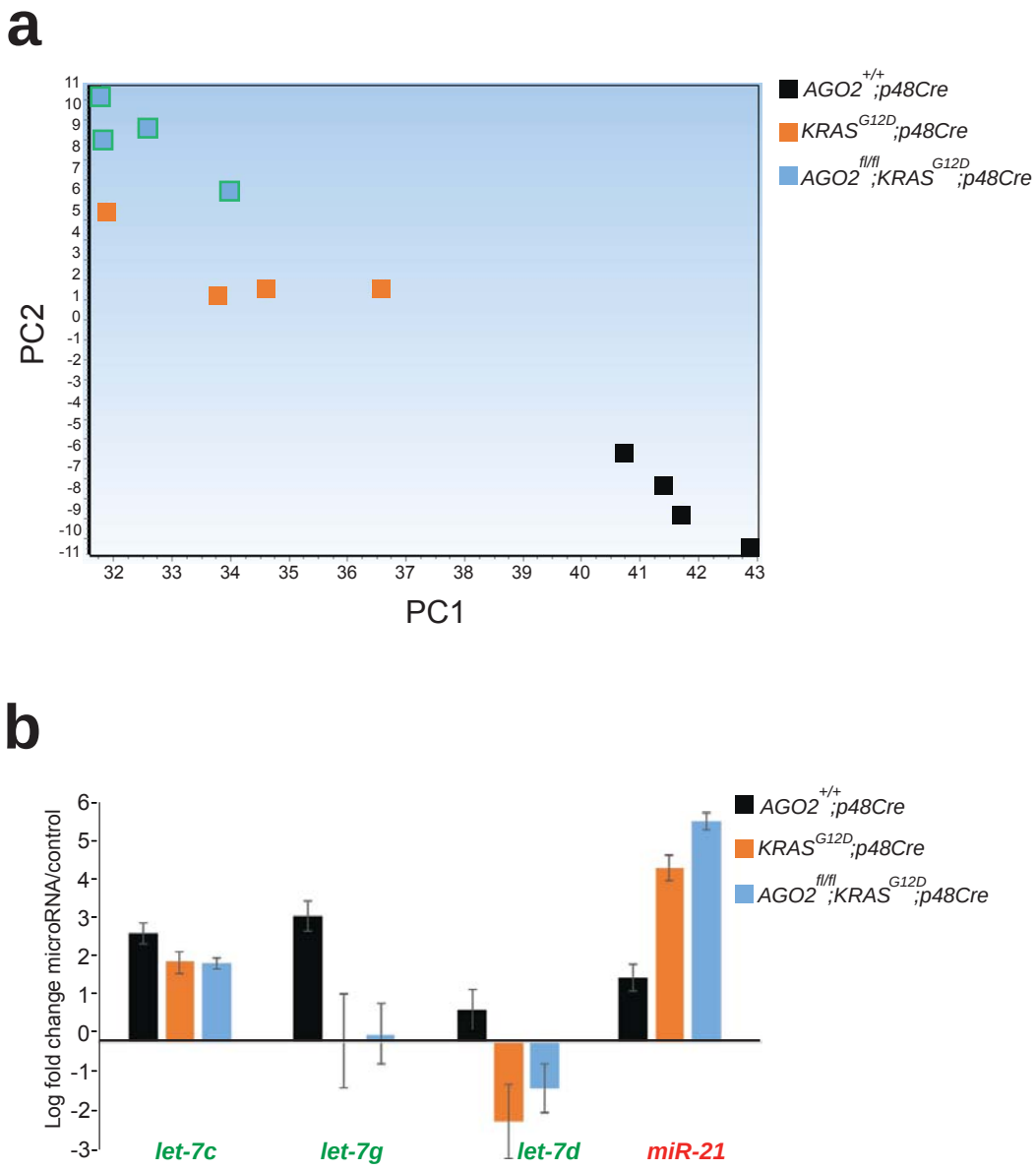

Extended Data Figure 8: AGO2 mediated RISC activity is not required to initiate mutant KRAS driven transformation. (**a**) Principal Component Analysis (PCA) of the differentially regulated microRNAs from pancreata obtained from 12 week old mice of the indicated genotypes. miRCURY LNA microRNA RT-qPCR (Qiagen) analysis was performed to determine relative expression of 334 microRNAs. GenEx ver 6 software was used for analysis of data obtained from qPCR analysis. (**b**) microRNA RT-qPCR analysis (miRCURY LNA, Qiagen) of select microRNAs obtained from pancreata from 12 week old mice with *AGO2*$^{+/+}$*;p48Cre*, *KRAS*^{G12D}*;p48Cre* and *AGO2*$^{fl/fl}$*;KRAS*^{G12D}*;p48Cre* genotypes. Median values (with p values below 0.001) obtained from four animals in each group are represented. Error bars represent SEM.

bioRxiv preprint doi: https://doi.org/10.1101/227264; this version posted November 30, 2017. The copyright holder for this preprint (which was not certified by peer review) is the author/funder, who has granted bioRxiv a license to display the preprint in perpetuity. It is made available under aCC-BY 4.0 International license.

Extended Data Figure 9

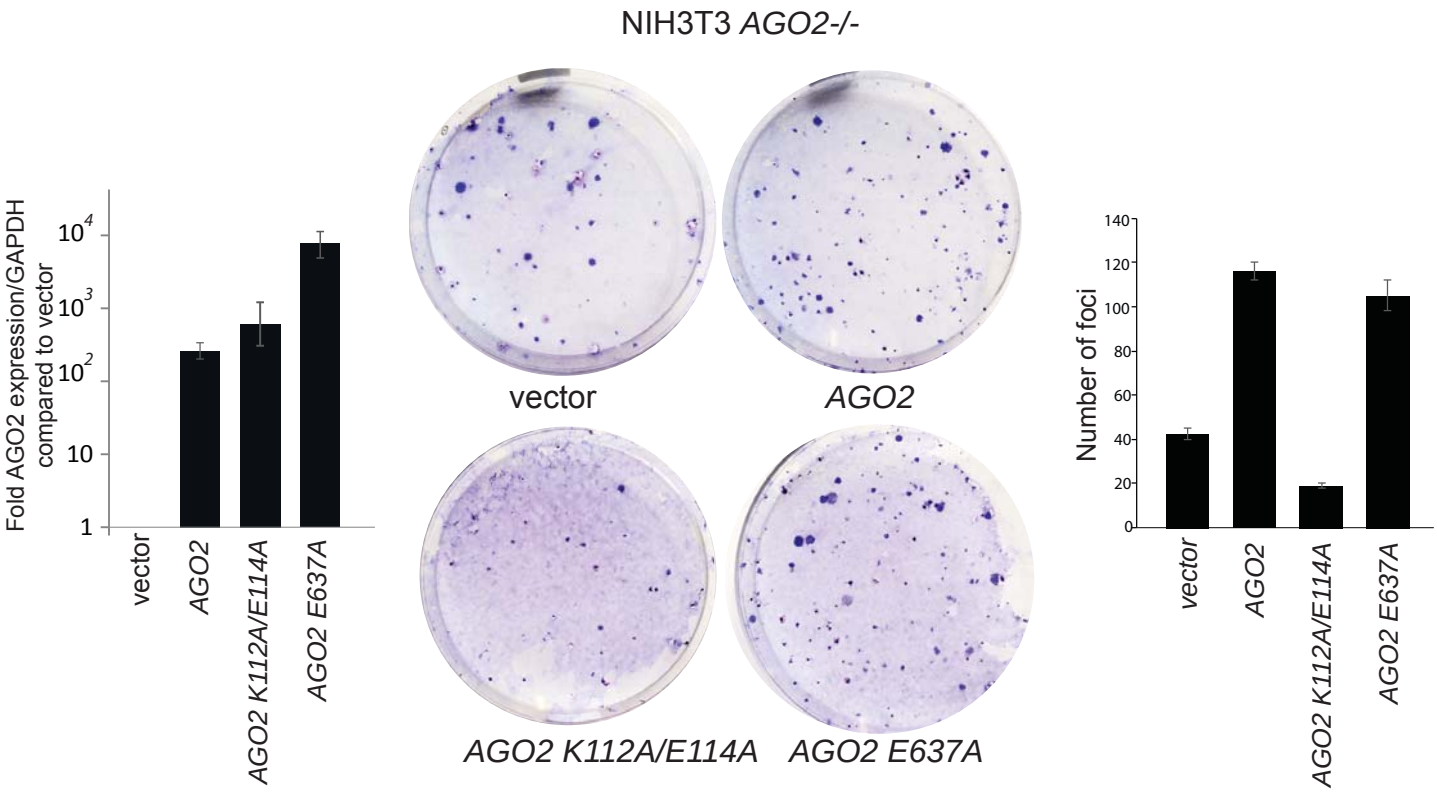

Extended Data Figure 9: Foci formation assay in NIH3T3 *AGO2-/-* cells using oncogenic KRAS co-expressed with different *AGO2* mutants (KRAS-binding deficient (*K112A/E114A*) and slicing deficient *E637A*). Left, Histogram shows the transcript levels of the different constructs measured by RT-qPCR. Center, representative plates showing foci obtained using the indicated constructs. Right, Histogram shows the number of foci in each group. Data shown is an average of two replicates. Error bars indicate SEM.

bioRxiv preprint doi: https://doi.org/10.1101/227264; this version posted November 30, 2017. The copyright holder for this preprint (which was not certified by peer review) is the author/funder, who has granted bioRxiv a license to display the preprint in perpetuity. It is made available under aCC-BY 4.0 International license.

Extended Data Figure 10

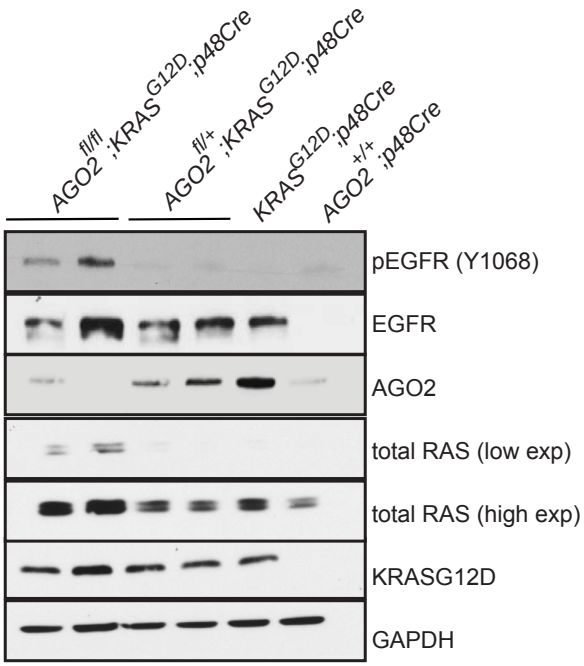

Extended Data Figure 10: Immunoblot analysis of AGO2 and associated RAS signaling molecules from individual pancreas obtained from 12 week old mice of the indicated genotypes.

bioRxiv preprint doi: https://doi.org/10.1101/227264; this version posted November 30, 2017. The copyright holder for this preprint (which was not certified by peer review) is the author/funder, who has granted bioRxiv a license to display the preprint in perpetuity. It is made available under aCC-BY 4.0 International License.

Extended Data Figure 11

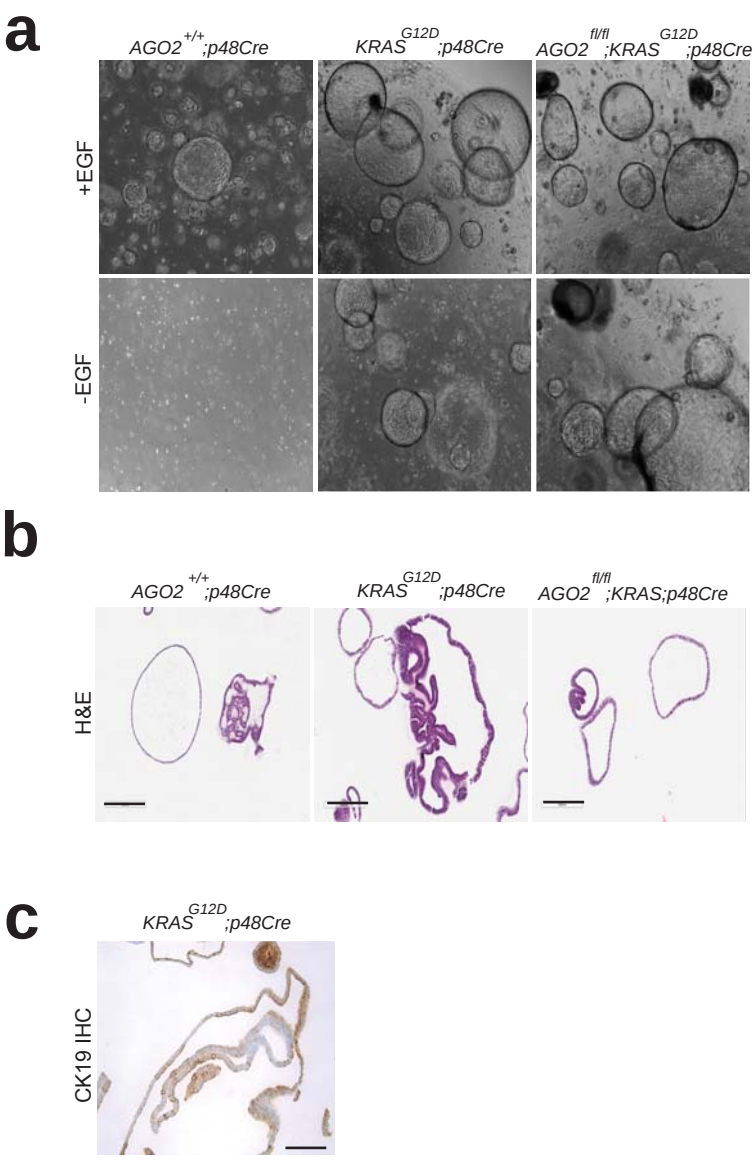

Extended Data Figure 11: Characterization of pancreatic ductal organoids obtained from 12 week old *KRAS^{G12D};p48Cre* and *AGO2$^{fl/fl}$;KRAS^{G12D};p48Cre* mice. (**a**) Light microscopic images of mouse pancreatic ductal organoids obtained from the indicated genotypes and cultured in the presence or absence of EGF. (**b**) H&E staining of pancreatic ductal organoids. Scale bar,200μm (*c*) CK19 (ductal marker) IHC staining of pancreatic ducts isolated from *KRAS^{G12D};p48Cre* mouse. Scale bar, 100μm.

bioRxiv preprint doi: https://doi.org/10.1101/227264; this version posted November 30, 2017. The copyright holder for this preprint (which was not certified by peer review) is the author/funder, who has granted bioRxiv a license to display the preprint in perpetuity. It is made available under aCC-BY 4.0 International license.

Extended Data Figure 12

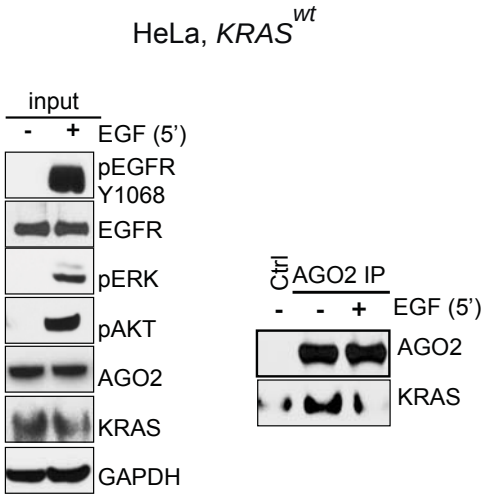

Extended Data Figure 12: IP of endogenous AGO2 upon EGF stimulation (5'), in HeLa (*KRAS*^{wt}) cells followed by immunoblot analysis of KRAS. Input blots on the left show MAPK activation and levels of various proteins.

bioRxiv preprint doi: https://doi.org/10.1101/227264; this version posted November 30, 2017. The copyright holder for this preprint (which was not certified by peer review) is the author/funder, who has granted bioRxiv a license to display the preprint in perpetuity. It is made available under aCC-BY 4.0 International license.

Table 1: Antibodies used for Immunoprecipitation and Immunobloting

#	Antibody	Vendor	Catalog Number	Application	Specificity	RAS antibody Validation
1	Anti-Ras clone 10 (RAS10)	Millipore	05-516	IP, IB, IF	Hu and Ms	Waters et al., 2017
2	K-Ras-2B Antibody (C-19)	Santa Cruz	sc-521	IP	Hu	Waters et al., 2017
3	K-Ras monoclonal Ab	Santa Cruz	sc-30	IB	human, mouse	Waters et al., 2017
4	KRAS-2B Antibody	Thermo Fisher S	415700	IF	human, mouse, rat	N/A
5	RAS (G12D Mutant Specific) DH87	Cell Signaling	14429S	IB	human	Waters et al., 2017
6	AGO2, 11A9	Sigma	SAB4200085	IP, IB	human	N/A
7	AGO2 EIF2C2	Sino Biologicals	11079-T36	IB, IHC, IF	human	N/A
8	Anti- EGFR (phospho Y1092)	Abcam	ab40815 (EP774Y)	IHC	human, mouse	
9	Phospho-EGF Receptor (Tyr1068)	Cell Signaling	2234S	IB	human, mouse	N/A
10	Phospho-p44/42 MAPK (Erk 1/2)	Cell Signaling	4376	IB	human, mouse	N/A
11	EGFR Antibody	Abcam	ab52894 (EP38Y)	IB,IHC	human, mouse, rat	
12	EGFR Antibody (A-10)	Santa Cruz	sc-373746	IB	human, mouse	N/A
13	Anti-FLAG antibody	Sigma	F7425-0.2MG	IB	human, mouse	N/A
14	Phospho-Akt S473	Cell Signaling	4060S	IB	human,mouse	N/A
15	Anti-Cytokeratin 19 antibody	Abcam	ab133496	IHC	mouse	
16	GAPDH-HRP	Cell Signaling	3683	IB	human, mouse	N/A
17	Normal Mouse IgG	Santa Cruz	sc-2025	Isotype Control IP	mouse	N/A
18	Normal Rat IgG	Abcam	ab18450	Isotype Control IP	rat	N/A
19	Normal Rabbit IgG	Millipore	12-370	Isotype Control IP	rabbit	N/A

IP: Immunoprecipitation; IB: Immunoblot; IHC: Immunohistochemistry

bioRxiv preprint doi: https://doi.org/10.1101/227264; this version posted November 30, 2017. The copyright holder for this preprint (which was not certified by peer review) is the author/funder, who has granted bioRxiv a license to display the preprint in perpetuity. It is made available under aCC-BY 4.0 International license.

Table 2: **Cases in *KRAS*^{G12D};*AGO2fl/fl;p48Cre* cohort with abnormal pathologies or death prior to 500 day time point**

Ear tag#	3331	2430	2385
Age (days)	368	500	500
Liver			
Ascites			
Lungs			
Diaphragm			
Hemorrhage			
Lymph nodes			
Kidneys			
Jaundice			
Enlarged Spleen			
Pathological Evaluation			
PDAC	no anaplastic PDAC or PDAC	no PDAC	no PDAC
Pancreas	low grade PanINs and cyst	only low grade PanIN	only low grade PanIN
AGO2 expression in pancreas	No AGO2 expression in the cyst or PanINs	no AGO2 expression in early PanINs	no AGO2 expression in early PanINs
Pancreatic Cyst	Yes	No cyst	No cyst
Further comment/ other pathology	resembles mucinous cystic neoplasm	likely benign lesion in lung, unknown origin	likely benign lesion in lung, unknown origin
AGO2 expression in mets?	n/a	AGO2 expressed in benign lung lesion	AGO2 expressed in benign lung lesion
Cause of Death	unknown	not dead before 500 days	not dead before 500 days

bioRxiv preprint doi: https://doi.org/10.1101/227264; this version posted November 30, 2017. The copyright holder for this preprint (which was not certified by peer review) is the author/funder, who has granted bioRxiv a license to display the preprint in perpetuity. It is made available under aCC-BY 4.0 International license.

Table 3: Primers used in the study

Transcript	Primer Sequence
m*HRAS*_Fwd	*5' GCTTCCTCTGTGTATTTGCCA 3'*
m*HRAS*_Rev	*5' CTTTCACCCGCTTGATCTGC 3'*
m*KRAS*_Fwd	*5' GTTAGCTCCAGTGCCCCAAT 3'*
m*KRAS*_Rev	*5' ATTCCCTAGGTCAGCGCAAC 3'*
m*NRAS*_Fwd	*5'ACTGGCCAAGAGTTACGGAA 3'*
m*NRAS*_Rev	*5' TGGCGTATCTCCCTTACCAG 3'*
m*AGO2*_Fwd	*5'GATCGCCAAGAGGAGATCAG3'*
m*AGO2*_Rev	*5'GCCTCCCAGTTTGACATTGA3'*
m*GAPDH*_Fwd	*5' AAGGTCATCCCAGAGCTGAA 3'*
m*GAPDH*_Rev	*5' CTGCTTCACCACCTTCTTGA 3'*

bioRxiv preprint doi: https://doi.org/10.1101/227264; this version posted November 30, 2017. The copyright holder for this preprint (which was not certified by peer review) is the author/funder, who has granted bioRxiv a license to display the preprint in perpetuity. It is made available under aCC-BY 4.0 International license.

Table 4: Cell Lines used in the study

Number	Cell Line	Source	Tissue	Type	*KRAS* or *AGO2* Status
1	HEK293	Human	Embryonic Kidney	Benign	*KRAS* WT
2	MCF-7	Human	Breast	Cancer	*KRAS* WT
3	HeLa	Human	Cervix	Cancer	*KRAS* WT
4	A375	Human	Skin Melanoma	Cancer	*KRAS* WT
5	PC3	Human	Prostate	Cancer	*KRAS* WT
6	A549	Human	Lung	Cancer	*KRAS* G12S
7	Capan-1	Human	Pancreas	Cancer	*KRAS* G12V
8	MIA PaCa-2	Human	Pancreas	Cancer	*KRAS* G12C
9	DLD-1	Human	Colorectal	Cancer	*KRAS* G13D
10	MEF, parental	Mouse	Embryonic Fribroblast	Benign	*AGO2 WT*
11	MEF, *AGO2* -/-	Mouse	Embryonic Fribroblast	Benign	*AGO2* Knockout
12	MEF, *AGO2* -/- ; + *AGO2*	Mouse	Embryonic Fribroblast	Benign	MEF *AGO2*-/- + *AGO2* rescue